

CHAPTER 4

Sensor Signal Conditioning

- Section 4-1: Introduction
- Section 4-2: Bridge Circuits
- Section 4-3: Strain, Force, Pressure and Flow Measurements
- Section 4-4: High Impedance Sensors
- Section 4-5: Temperature Sensors

Sensor Signal Conditioning

Walt Kester, James Bryant, Walt Jung

Scott Wurcer, Chuck Kitchin

SECTION 4-1

Introduction

Walt Kester

This chapter of the book deals with various sensors and associated signal-conditioning circuitry involving the use of op amps and in amps. While the topic is generally very broad, the focus is to concentrate on circuit and signal processing applications of sensors rather than the details of the actual sensors themselves.

Strictly speaking, a *sensor* is a device that receives a signal or stimulus and responds with an electrical signal, while a *transducer* is a converter of one type of energy into another. In practice, however, the terms are often used interchangeably.

Sensors and their associated circuits are used to measure various physical properties such as temperature, force, pressure, flow, position, light intensity, and so forth. These properties act as the stimulus to the sensor, and the sensor output is conditioned and processed to provide the corresponding measurement of the physical property. We will not cover all possible types of sensors, only the most popular ones, and specifically, those that lend themselves to process control and data acquisition systems.

Sensors do not operate by themselves. They are generally part of a larger system consisting of signal conditioners and various analog or digital signal processing circuits. The *system* could be a measurement system, data acquisition system, or process control system, for example.

Sensors may be classified in a number of ways. From a signal-conditioning viewpoint it is useful to classify sensors as either *active* or *passive*. An *active* sensor requires an external source of excitation. Resistor-based sensors such as thermistors, resistance temperature detectors (RTDs), and strain gages are examples of active sensors, because a current must be passed through them and the corresponding voltage measured in order to determine the resistance value. An alternative would be to place the devices in a bridge circuit; however in either case, an external current or voltage is required.

On the other hand, *passive* (or *self-generating*) sensors generate their own electrical output signal without requiring external voltages or currents. Examples of passive sensors are thermocouples and photodiodes which generate thermoelectric voltages and photocurrents, respectively, which are independent of external circuits.

It should be noted that these definitions (*active* versus *passive*) refer to the need (or lack thereof) of external active circuitry to produce a sensor electrical output signal. It would seem equally logical to consider a thermocouple *active*, in the sense that it produces an output voltage without external circuitry; however the convention in the industry is to classify the sensor with respect to the external circuit requirement as defined above.

A logical way to classify sensors is with respect to the physical property the sensor is designed to measure. Thus we have temperature sensors, force sensors, pressure sensors, motion sensors, and so forth. However, sensors that measure different properties may have the same type of electrical output. For instance, Resistance Temperature Detector (RTD) is a variable resistance, as is a resistive strain gage. Both RTDs and strain gages are often placed in bridge circuits, and the conditioning circuits are therefore quite similar. In fact, bridges and their conditioning circuits deserve a detailed discussion. Figure 4-1 is an overview of basic sensor characteristics.

- Sensors:
Convert a Signal or Stimulus (Representing a Physical Property) into an Electrical Output
- Transducers:
Convert One Type of Energy into Another
- The Terms are often Interchanged
- Active Sensors Require an External Source of Excitation:
RTDs, Strain-Gages
- Passive (Self-Generating) Sensors do not:
Thermocouples, Photodiodes

Figure 4-1: An overview of sensor characteristics

The full-scale outputs of most sensors (passive or active) are relatively small voltages, currents, or resistance changes, and therefore their outputs must be properly conditioned before further analog or digital processing can occur. Because of this, an entire class of circuits has evolved, generally referred to as signal-conditioning circuits. Amplification, level translation, galvanic isolation, impedance transformation, linearization, and filtering are fundamental signal-conditioning functions that may be required. Figure 4-2 summarizes sensors and their outputs.

PROPERTY	SENSOR	ACTIVE/ PASSIVE	OUTPUT
Temperature	Thermocouple Silicon RTD Thermistor	Passive Active Active Active	Voltage Voltage/Current Resistance Resistance
Force / Pressure	Strain Gage Piezoelectric	Active Passive	Resistance Voltage
Acceleration	Accelerometer	Active	Capacitance
Position	LVDT	Active	AC Voltage
Light Intensity	Photodiode	Active	Current

Figure 4-2: Typical sensors and their output formats

Whatever form the conditioning takes, the circuitry and performance will be governed by the electrical character of the sensor and its output. Accurate characterization of the sensor in terms of parameters appropriate to the application, e.g., sensitivity, voltage and current levels, linearity, impedances, gain, offset, drift, time constants, maximum electrical ratings, stray impedances, and other important considerations can spell the difference between substandard and successful application of the device, especially where high resolution, precision, or low level measurements are necessary.

Higher levels of integration now allow ICs to play a significant role in both analog and digital signal conditioning. ADCs specifically designed for measurement applications often contain on-chip programmable-gain amplifiers (PGAs) and other useful circuits, such as current sources for driving RTDs, thereby minimizing the external conditioning circuit requirements.

To some degree or another, most sensor outputs are nonlinear with respect to the applied stimulus and as a result, their outputs must often be linearized in order to yield correct measurements. In terms of the design approach choice towards linearization, the designer can take a route along either of two major paths.

Analog is one viable route, and such techniques may be used to perform an “analog domain” linearization function.

However, the recent introduction of high performance ADCs now allows linearization to be done much more efficiently and accurately in software. This “digital domain” approach to linearization eliminates the need for tedious manual calibration using multiple and sometimes interactive analog trim adjustments.

A quite common application of sensors is within process control systems. One example would be control of a physical property, such as temperature. A sample block diagram of how this might be implemented is illustrated in Figure 4-3.

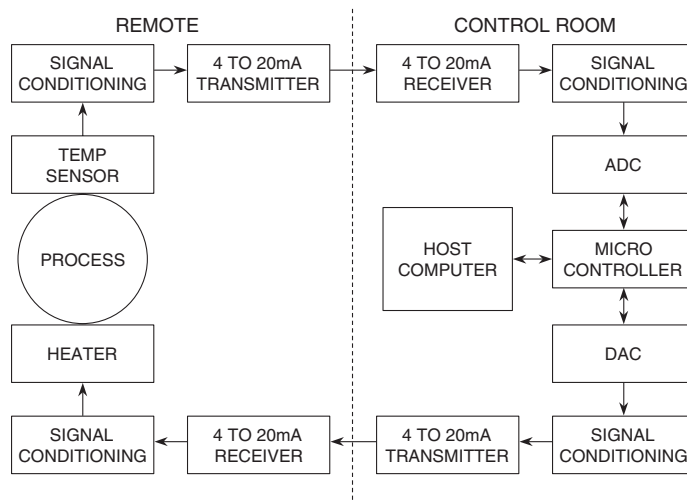


Figure 4-3: A typical industrial process temperature control loop

In this system, an output from a temperature sensor is conditioned, transmitted over some distance, received, and then digitized by an ADC. The microcontroller or host computer determines if the temperature is above or below the desired value, and outputs a digital word to the digital-to-analog converter (DAC).

The DAC output is conditioned and drives the remotely located *actuator*, in this case a heater. Notice that the interface between the control center and the remote process is via the industry-standard 4-20 mA loop.

Digital techniques are becoming more and more popular in processing sensor outputs in data acquisition, process control, and measurement. 8-bit microcontrollers (8051-based, for example) generally have sufficient speed and processing capability for most applications.

By including the A/D conversion and the microcontroller programmability on the sensor itself, a “smart sensor” can be implemented with self-contained calibration and linearization features among others. However, such digital techniques aren’t a major focus of this text, so the section references may be consulted for further information.

The remaining sections of the chapter deal with analog signal conditioning methods for a variety of sensor types.

References: Introduction

1. Walt Kester, Bill Chestnut, and Grayson King, *Smart Sensors*, Chapter 9 of **Practical Design Techniques for Sensor Signal Conditioning**, Analog Devices, Inc., 1999, ISBN: 0-916550-20-6.
2. Compatibility of Analog Signals for Electronic Industrial Process Instruments, ANSI/ISA-S50.1-1982 (Rev. 1992), www.isa.org.
3. Editors, “Fieldbuses: Look Before You Leap,” **EDN**, November 5, 1998, p. 197.
4. “MicroConverter Technology Backgrounder,” Whitepaper, Analog Devices, Inc., www.analog.com.
5. Scott MacKenzie, **The 8051 Microcontroller, 3rd Ed.**, Prentice-Hall, 1999, ISBN: 0-13-780008-8.

Bridge Circuits

Walt Kester

An Introduction to Bridges

This section of the chapter, 4-2, discusses more fundamental bridge circuit concepts. To gain greatest appreciation of these ideas, it should be studied along with those sections discussing precision op amps within Chapters 1 and 2. The next section (4-3) focuses on the detailed application circuits relating to strain-gage-based sensors. These sections can be read sequentially if the reader already understands the design issues related to precision op amp applications.

Resistive elements are some of the most common sensors. They are inexpensive, and relatively easy to interface with signal-conditioning circuits. Resistive elements can be made sensitive to temperature, strain (by pressure or by flex), and light. Using these basic elements, many complex physical phenomena can be measured, such as: fluid or mass flow (by sensing the temperature difference between two calibrated resistances), dew-point humidity (by measuring two different temperature points), and so forth.

Sensor element resistance can range from less than 100 Ω to several hundred k Ω , depending on the sensor design and the physical environment to be measured. Figure 4-4 indicates the wide range of sensor resistance encountered. For example, RTDs are typically 100 Ω or 1000 Ω . Thermistors are typically 3500 Ω or higher.

• Strain Gages	120 Ω , 350 Ω , 3500 Ω
• Weigh-Scale Load Cells	350 Ω – 3500 Ω
• Pressure Sensors	350 Ω – 3500 Ω
• Relative Humidity	100k Ω – 10M Ω
• Resistance Temperature Devices (RTDs)	100 Ω , 1000 Ω
• Thermistors	100 Ω – 10M Ω

Figure 4-4: Sensor resistances used in bridge circuits span a wide dynamic range

Resistive sensors such as RTDs and strain gages produce relatively small percentage changes in resistance, in response to a change in a physical variable such as temperature or force. For example, platinum RTDs have a temperature coefficient of about 0.385%/°C. Thus, in order to accurately resolve temperature to 1°C, the overall measurement accuracy must be much better than 0.385 Ω when using a 100 Ω RTD.

Strain gages present a significant measurement challenge because the typical change in resistance over the entire operating range of a strain gage may be less than 1% of the nominal resistance value. Accurately measuring small resistance changes is therefore critical when applying resistive sensors.

A simple method for measuring resistance is to force a constant current through the resistive sensor, and measure the voltage output. This requires both an accurate current source and an accurate means of measuring the voltage. Any change in the current will be interpreted as a resistance change. In addition, the power dissipation in the resistive sensor must be small and in accordance with the manufacturer's recommendations, so that self-heating does not produce errors. As a result, the drive current must be small, which tends to limit the resolution of this approach.

A *resistance bridge*, shown in Figure 4-5, offers an attractive alternative for accurately measuring small resistance changes. This is a basic Wheatstone bridge (actually developed by S. H. Christie in 1833), and is a prime example. It consists of four resistors connected to form a quadrilateral, a source of excitation voltage V_B (or, alternately, a current) connected across one of the diagonals, and a voltage detector connected across the other diagonal. The detector measures the difference between the outputs of the two voltage dividers connected across the excitation voltage, V_B . The general form of the bridge output V_O is noted in the figure.

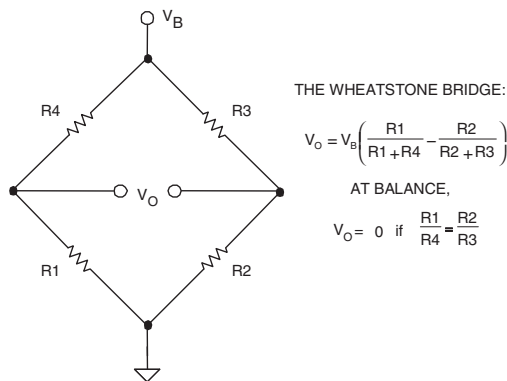


Figure 4-5: The basic Wheatstone bridge produces an output null when the ratios of sidearm resistances match

There are two principal ways of operating a bridge such as this. One is by operating it as a null detector, where the bridge measures resistance indirectly by comparison with a similar standard resistance. On the other hand, it can be used as a device that reads a resistance difference directly, as a proportional voltage output.

When $R_1/R_4 = R_2/R_3$, the resistance bridge is said to be at a *null*, irrespective of the mode of excitation (current or voltage, ac or dc), the magnitude of excitation, the mode of readout (current or voltage), or the impedance of the detector. Therefore, if the ratio of R_2/R_3 is fixed at K , a null is achieved when $R_1 = K \cdot R_4$. If R_1 is unknown and R_4 is an accurately determined variable resistance, the magnitude of R_1 can be found by adjusting R_4 until an output null is achieved. Conversely, in sensor-type measurements, R_4 may be a fixed reference, and a null occurs when the magnitude of the external variable (strain, temperature, and so forth.) is such that $R_1 = K \cdot R_4$.

Null measurements are principally used in feedback systems involving electromechanical and/or human elements. Such systems seek to force the active element (strain gage, RTD, thermistor, and so forth.) to balance the bridge by influencing the parameter being measured.

For the majority of sensor applications employing bridges, however, the deviation of one or more resistors in a bridge from an initial value is measured as an indication of the magnitude (or a change) in the measured variable. In these cases, the output voltage change is an indication of the resistance change. Because very small resistance changes are common, the output voltage change may be as small as tens of millivolts, even with the excitation voltage $V_B = 10\text{ V}$ (typical for a load cell application).

In many bridge applications, there may not just be a single variable element, but two, or even four elements, all of which may vary. Figure 4-6 shows a family of four voltage-driven bridges, those most commonly suited for sensor applications. In the four cases the corresponding equations for V_O relate the bridge output voltage to the excitation voltage and the bridge resistance values. In all cases we assume a constant voltage drive, V_B . Note that since the bridge output is always directly proportional to V_B , the measurement accuracy can be no better than that of the accuracy of the excitation voltage.

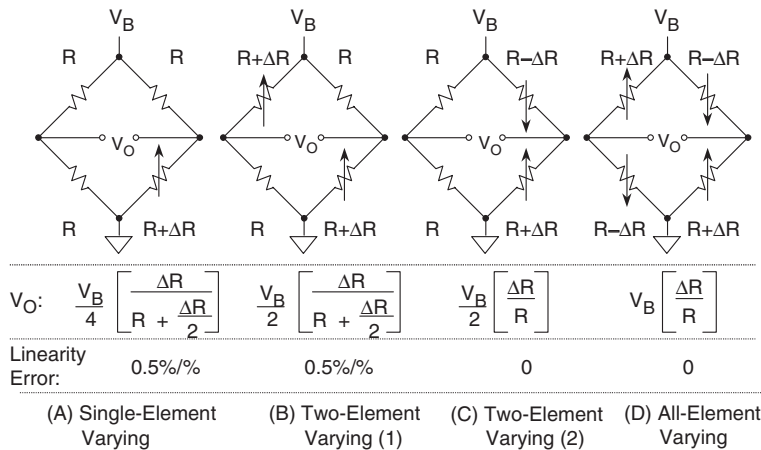


Figure 4-6: The output voltage sensitivity and linearity of constant voltage drive bridge configurations differs according to the number of active elements

In each case, the value of the fixed bridge resistor “R” is chosen to be equal to the nominal value of the variable resistor(s). The deviation of the variable resistor(s) about the nominal value is assumed to be proportional to the quantity being measured, such as strain (in the case of a strain gage), or temperature (in the case of an RTD).

The *sensitivity* of a bridge is the ratio of the maximum expected change in the output voltage to the excitation voltage. For instance, if $V_B = 10\text{ V}$, and the full-scale bridge output is 10mV, then the sensitivity is 1mV/V. For the four cases of Figure 4-6, sensitivity can be said to increase going left-right, or as more elements are made variable.

The *single-element varying* bridge of Figure 4-6A is most suited for temperature sensing using RTDs or thermistors. This configuration is also used with a single resistive strain gage. All the resistances are nominally equal, but one of them (the sensor) is variable by an amount ΔR . As the equation indicates, the relationship between the bridge output and ΔR is not linear. For example, if $R = 100\ \Omega$ and $\Delta R = 0.1\ \Omega$ (0.1% change in resistance), the output of the bridge is 2.49875 mV for $V_B = 10\text{ V}$. The error is 2.50000 mV – 2.49875 mV, or 0.00125 mV. Converting this to a % of full-scale by dividing by 2.5 V yields an end-point linearity error in percent of approximately 0.05%. (Bridge end-point linearity error is

calculated as the worst error in % FS from a straight line which connects the origin and the end point at FS, i.e., the FS gain error is not included). If $\Delta R = 1 \Omega$, (1% change in resistance), the output of the bridge is 24.8756 mV, representing an end-point linearity error of approximately 0.5%. The end-point linearity error of the single-element bridge can be expressed in equation form:

Single-Element Varying

$$\text{Bridge End-Point Linearity Error} \approx \% \text{ Change in Resistance} \div 2$$

It should be noted that the above nonlinearity refers to the nonlinearity of the bridge itself and not the sensor. In practice, most sensors themselves will exhibit a certain specified amount of nonlinearity, which must also be accounted for in the final measurement.

In some applications, the bridge nonlinearity noted above may be acceptable. If not, there are various methods available to linearize bridges. Since there is a fixed relationship between the bridge resistance change and its output (shown in the equations), software can be used to remove the linearity error in digital systems. Circuit techniques can also be used to linearize the bridge output directly, and these will be discussed shortly.

There are two cases to consider in the instance of a *two-element varying* bridge. In Case 1 (Figure 4-6B), both of the diagonally opposite elements change in the same direction. An example would be two identical strain gages mounted adjacent to each other, with their axes in parallel.

The nonlinearity for this case, 0.5%/%, the same as that of the single-element varying bridge of Figure 4-6A. However, it is interesting to note the sensitivity is now improved by a factor of 2, vis-à-vis the single-element varying setup. The two-element varying bridge is commonly found in pressure sensors and flow meter systems.

A second case of the two-element varying bridge, Case 2, is shown in Figure 4-6C. This bridge requires two identical elements that vary in *opposite* directions. This could correspond to two identical strain gages: one mounted on top of a flexing surface, and one on the bottom. Note that this configuration is now linear, and like two-element varying Case 1, it has twice the sensitivity of the Figure 4-6A configuration. Another way to view this configuration is to consider the terms $R + \Delta R$ and $R - \Delta R$ as comprising two sections of a linear potentiometer.

The *all-element varying* bridge of Figure 4-6D produces the most signal for a given resistance change, and is inherently linear. It is also an industry-standard configuration for load cells constructed from four identical strain gages. Understandably, it is also one of the most popular bridge configurations.

Bridges may also be driven from constant current sources, as shown in Figure 4-7, for the corresponding cases of single, dual, dual, and four active element(s). As with the voltage-driven bridges, the analogous output expressions are noted, along with the sensitivities.

Current drive, although not as popular as voltage drive, does have advantages when the bridge is located remotely from the source of excitation. One advantage is that the wiring resistance doesn't introduce errors in the measurement; another is simpler, less expensive cabling. Note also that with constant current excitation, all bridge configurations are linear except the single-element varying case of Figure 4-7A.

In summary, there are many design issues relating to bridge circuits, as denoted by Figure 4-8. After selecting the basic configuration, the excitation method must be determined. The value of the excitation voltage or current must first be determined, as this directly influences sensitivity. Recall that the full-scale bridge output is directly proportional to the excitation voltage (or current). Typical bridge sensitivities are 1mV/V to 10mV/V.

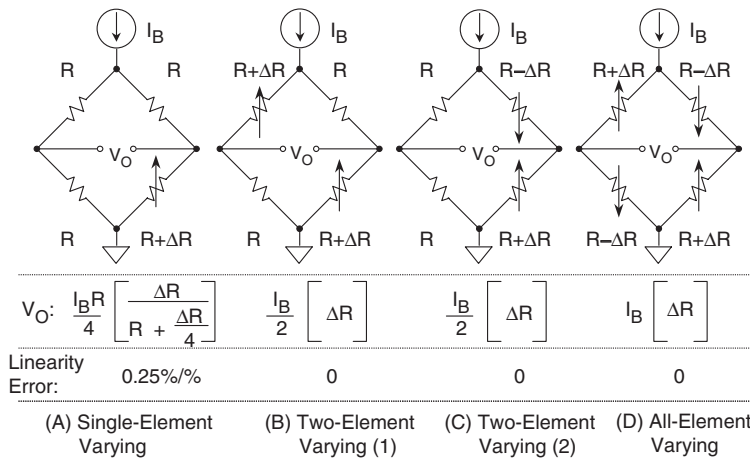


Figure 4-7: The output voltage sensitivity and linearity of constant current drive bridge configurations also differs according to the number of active elements

- Selecting Configuration (1-, 2-, 4-Element Varying)
- Selection of Voltage or Current Excitation
- Ratiometric Operation
- Stability of Excitation Voltage or Current
- Bridge Sensitivity: FS Output / Excitation Voltage
1mV/V to 10mV/V Typical
- Full-scale Bridge Outputs: 10mV – 100mV Typical
- Precision, Low Noise Amplification/Conditioning Techniques Required
- Linearization Techniques May Be Required
- Remote Sensors Present Challenges

Figure 4-8: A number of bridge considerations impact design choices

Although large excitation voltages yield proportionally larger full-scale output voltages, they also result in higher bridge power dissipation, and thus raise the possibility of sensor resistor self-heating errors. On the other hand, low values of excitation voltage require more gain in the conditioning circuits, and also increase sensitivity to low level errors such as noise and offset voltages.

Regardless of the absolute level, the stability of the excitation voltage or current directly affects the overall accuracy of the bridge output, as is evident from the V_B and I_B terms in the output expressions. Therefore stable references and/or *ratiometric* drive techniques are required, to maintain highest accuracy.

Here, ratiometric simply refers to the use of the bridge drive voltage of a voltage-driven bridge (or a current-proportional voltage, for a current-driven bridge) as the reference input to the ADC that digitizes the

amplified bridge output voltage. In this manner the absolute accuracy and stability of the excitation voltage becomes a second-order error. Examples to follow further illustrate this point.

Amplifying and Linearizing Bridge Outputs

The output of a single-element varying bridge may be amplified by a single precision op amp connected as shown in Figure 4-9. Unfortunately this circuit, although attractive because of relative simplicity, has poor overall performance. Its gain predictability and accuracy are poor, and it unbalances the bridge due to loading from R_F and the op amp bias current. The R_F resistors must be carefully chosen and matched to maximize common mode rejection (CMR). Also, it is difficult to maximize the CMR while at the same time allowing different gain options. Gain is dependent upon the bridge resistances and R_F . In addition, the output is nonlinear, as the configuration does nothing to address the intrinsic bridge nonlinearity. In summary, the circuit isn't recommended for precision use.

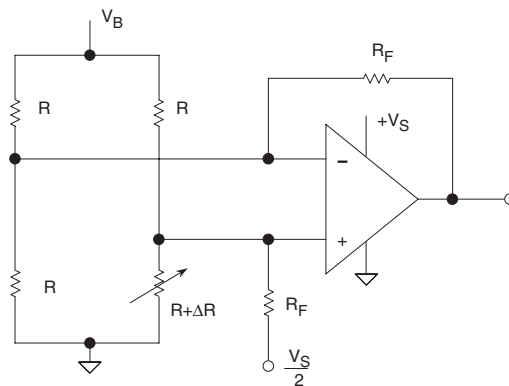


Figure 4-9: Using a single op amp as a bridge amplifier

However, a redeeming feature of this circuit is that it is capable of single supply operation, with a solitary op amp. Note that the R_F resistor connected to the noninverting input is returned to $V_S/2$ (rather than ground) so that both positive and negative ΔR values can be accommodated, with the bipolar op amp output swing referenced to $V_S/2$.

A much better approach is to use an *instrumentation amplifier* (in amp) for the required gain, as shown in Figure 4-10. This efficient circuit provides better gain accuracy, with the in amp gain usually set with a single resistor, R_G . Since the amplifier provides dual, high-impedance loading to the bridge nodes, it does not unbalance or load the bridge. Using modern in amp devices with gains ranging from 10–1000, excellent common mode rejection and gain accuracy can be achieved with this circuit.

However, due to the intrinsic characteristics of the bridge, the output is still nonlinear (see expression). As noted earlier, this can be corrected in software (assuming that the in amp output is digitized using an analog-to-digital converter and followed by a microcontroller or microprocessor).

The in amp can be operated on either dual supplies as shown, or alternately, on a single positive supply. In the figure, this corresponds to $-V_S = 0$. This is a key advantage, due to the fact that all such bridge circuits bias the in amp inputs at $V_B/2$, a voltage range typically compatible with amplifier bias requirements. In amps such as the AD620 family, the AD623, and AD627 can be used in single (or dual) supply bridge applications, provided their restrictions on the gain and input and output voltage swings are observed.

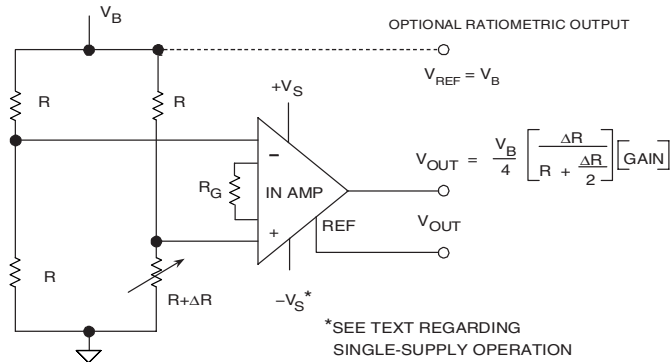


Figure 4-10: A generally preferred method of bridge amplification employs an instrumentation amplifier for stable gain and high CMR

The bridge in this example is voltage driven, by the voltage V_B . This voltage can optionally be used for an ADC reference voltage, in which case it also is an additional output, V_{REF} .

Various techniques are available to linearize bridge outputs, but it is important to distinguish between the linearity of the bridge equation (discussed earlier), and the sensor response linearity to the phenomenon being sensed. For example, if the active sensor element is an RTD, the bridge used to implement the measurement might have perfectly adequate linearity; *yet the output could still be nonlinear*, due to the RTD device's intrinsic nonlinearity. Manufacturers of sensors employing bridges address the nonlinearity issue in a variety of ways, including keeping the resistive swings in the bridge small, shaping complementary non-linear response into the active elements of the bridge, using resistive trims for first-order corrections, and others. In the examples which follow, what is being addressed is the linearity error of the bridge configuration itself (as opposed to a sensor element within the bridge).

Figure 4-11 shows a single-element varying active bridge circuit, in which an op amp produces a forced bridge null condition. For this single-element varying case, only the op amp feedback resistance varies, with the remaining three resistances fixed.

As used here, the op amp output provides a buffered, ground referenced, low impedance output for the bridge measurement, effectively suppressing the $V_B/2$ CM bridge component at the op amp inputs.

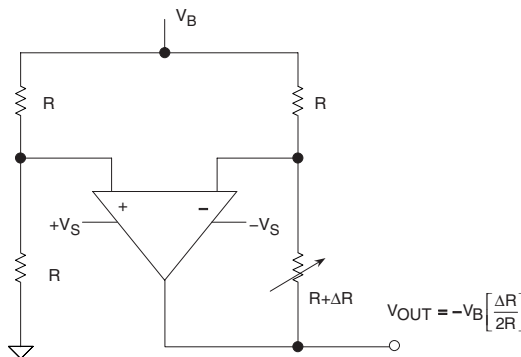


Figure 4-11: Linearizing a single-element varying bridge (Method 1)

The circuit works by adding a voltage in series with the variable resistance arm. This voltage is equal in magnitude and opposite in polarity to the incremental voltage across the varying element, and is linear with ΔR . As can be noted, the three constant “R” valued resistances and the op amp operate to drive a constant current in the variable resistance. This is the basic mechanism that produces the linearized output.

This active bridge has a sensitivity gain of two over the standard single-element varying bridge (Figure 4-6A). The key point is that the bridge’s incremental resistance/voltage output becomes linear, even for large values of ΔR . However, because of a still relatively small output signal, a second amplifier must usually follow this bridge. Note also that the op amp used in this circuit requires dual supplies, because its output must go negative for conditions where ΔR is positive.

Another circuit for linearizing a single-element varying bridge is shown in Figure 4-12. The top node of the bridge is excited by the voltage, V_B . The bottom of the bridge is driven in complementary fashion by the left op amp, which maintains a constant current of V_B/R in the varying resistance element, $R + \Delta R$.

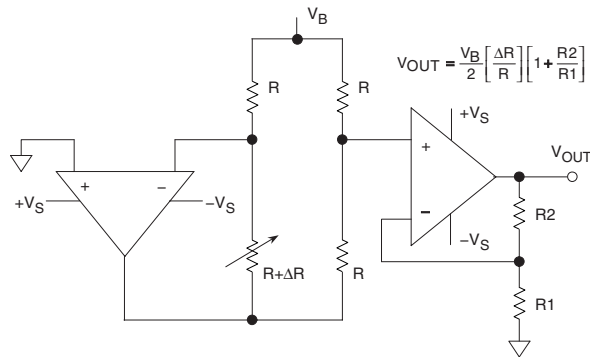


Figure 4-12: Linearizing a single-element varying bridge (Method 2)

Like the circuit of Figure 4-11, the constant current drive for the single-element variable resistance provides the mechanism for linearity improvement. Also, because of the fact that the bridge left-side center node is ground-referenced by the op amp, this configuration effectively suppresses CM voltages. This has the virtue of making the op amp selection somewhat less critical. Of course, performance parameters of high gain, low offset/noise, and high stability are all still needed.

The output signal is taken from the right-hand leg of the bridge, and is amplified by a second op amp, connected as a noninverting gain stage. With the scaling freedom provided by the second op amp, the configuration is very flexible. The net output is linear, and has a bridge-output referred sensitivity comparable to the single-element varying circuit of Figure 4-11.

The Figure 4-12 circuit requires two op amps operating on dual supplies. In addition, paired resistors R1-R2 must be ratio matched and stable types, for overall accurate and stable gain. The circuit can be a practical one using a dual precision op amp, such as an AD708, the OP2177 or the OP213.

A closely related circuit for linearizing a voltage-driven, *two-element* varying bridge can be adapted directly from the basic circuit of Figure 4-11. This form of the circuit, shown in Figure 4-13, is identical to the previous single-element varying case, with the exception that the resistance between V_B and the op amp (+) input is now also variable (i.e., both diagonal $R + \Delta R$ resistances vary, in a like manner).

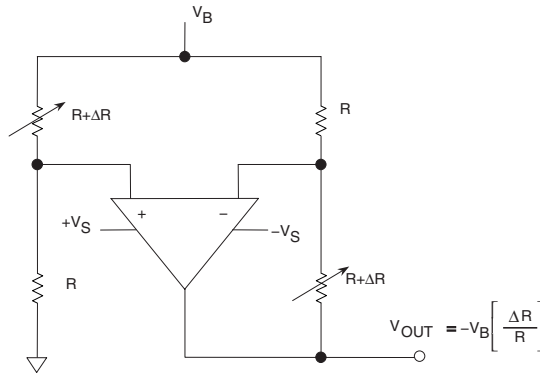


Figure 4-13: Linearizing a two-element varying voltage-driven bridge (Method 1)

For the same applied voltage V_B , this form of the circuit has twice the sensitivity, which is evident in the output expressions. A dual supply op amp is again required, and additional gain may also be necessary.

The two-element varying bridge circuit shown in Figure 4-14 uses an op amp, a sense resistor, and a voltage reference, set up in a feedback loop containing the sensing bridge. The net effect of the loop is to maintain a constant current through the bridge of $I_B = V_{REF}/R_{SENSE}$. The current through each leg of the bridge remains constant ($I_B/2$) as the resistances change, therefore the output is a linear function of ΔR . An in amp provides the additional gain.

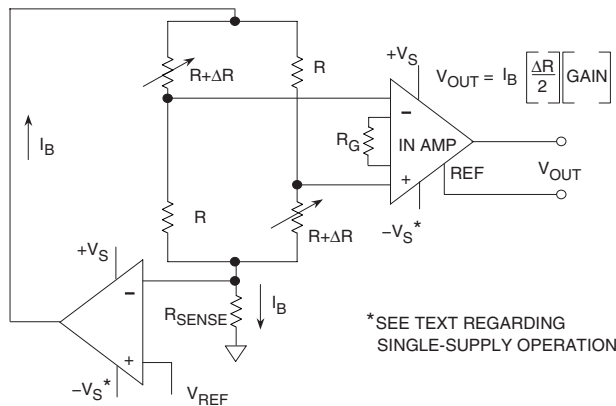


Figure 4-14: Linearizing a two-element varying current-driven bridge (Method 2)

This circuit can be operated on a single supply with the proper choice of amplifiers and signal levels. If ratiometric operation of an ADC is desired, the V_{REF} voltage can be used to drive the ADC.

Driving Remote Bridges

Wiring resistance and noise pickup are the biggest problems associated with remotely located bridges. Figure 4-15 shows a 350 Ω strain gage, which is connected to the rest of the bridge circuit by 100 feet of 30-gage twisted-pair copper wire. The resistance of the wire at 25°C is 0.105 Ω /ft, or 10.5 Ω for 100 ft. The total lead resistance in series with the 350 Ω strain gage is therefore 21 Ω . The temperature coefficient of the copper wire is 0.385%/°C. Now we will calculate the gain and offset error in the bridge output due to a 10°C temperature rise in the cable. These calculations are easy to make, because the bridge output voltage is simply the difference between the output of two voltage dividers, each driven from a 10 V source.

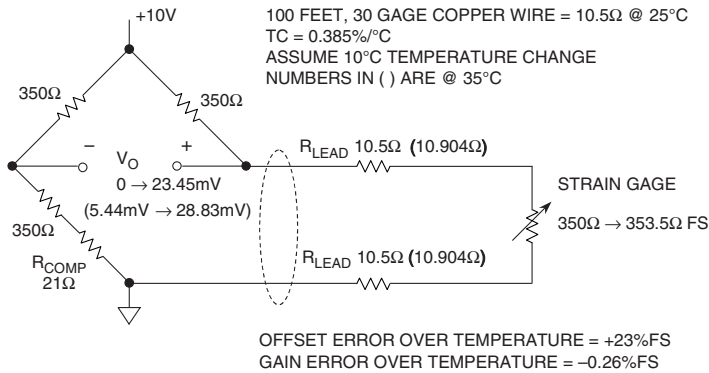


Figure 4-15: Wiring resistance related errors with remote bridge sensor

The full-scale variation of the strain gage resistance (with flex) above its nominal 350 Ω value is +1% (+3.5 Ω), corresponding to a full-scale strain gage resistance of 353.5 Ω which causes a bridge output voltage of +23.45 mV. Notice that the addition of the 21 Ω R_{COMP} resistor compensates for the wiring resistance and balances the bridge when the strain gage resistance is 350 Ω . Without R_{COMP}, the bridge would have an output offset voltage of 145.63 mV for a nominal strain gage resistance of 350 Ω . This offset could be compensated for in software just as easily but, for this example, we chose to do it with R_{COMP}.

Assume that the cable temperature increases 10°C above nominal room temperature. This results in a total lead resistance increase of +0.404 Ω (10.5 Ω × 0.00385/°C × 10°C) in each lead. *Note: The values in parentheses in the diagram indicate the values at 35°C.* The total additional lead resistance (of the two leads) is +0.808 Ω . With no strain, this additional lead resistance produces an offset of +5.44 mV in the bridge output. Full-scale strain produces a bridge output of +28.83 mV (a change of +23.39 mV from no strain). Thus the increase in temperature produces an offset voltage error of +5.44 mV (+23% full-scale) and a gain error of -0.06 mV (23.39 mV - 23.45 mV), or -0.26% full-scale. Note that these errors are produced solely by the 30-gage wire, and do not include any temperature coefficient errors in the strain gage itself.

The effects of wiring resistance on the bridge output can be minimized by the 3-wire connection shown in Figure 4-16. We assume that the bridge output voltage is measured by a high impedance device, therefore there is no current in the sense lead. Note that the sense lead measures the voltage output of a divider: the top half is the bridge resistor plus the lead resistance, and the bottom half is strain gage resistance plus the lead resistance. The nominal sense voltage is therefore independent of the lead resistance. When the strain gage resistance increases to full-scale (353.5 Ω), the bridge output increases to +24.15 mV.

Increasing the temperature to 35°C increases the lead resistance by +0.404 Ω in each half of the divider. The full-scale bridge output voltage decreases to +24.13 mV because of the small loss in sensitivity, but

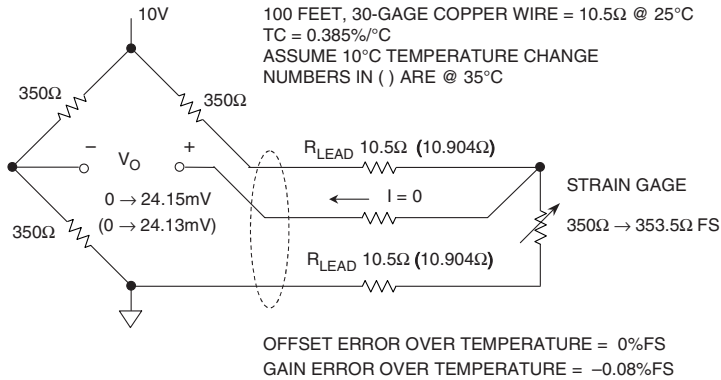


Figure 4-16: Remote bridge wiring resistance errors are reduced with 3-wire sensor connection

there is no offset error. The gain error due to the temperature increase of 10°C is therefore only -0.02 mV, or -0.08% of full-scale. Compare this to the +23% full-scale offset error and the -0.26% gain error for the 2-wire connection shown in Figure 4-14.

The 3-wire method works well for remotely located resistive elements which make up one leg of a single-element varying bridge. However, all-element varying bridges are generally housed in a complete assembly, as in the case of a load cell. When these bridges are remotely located from the conditioning electronics, special techniques must be used to maintain accuracy.

Of particular concern is maintaining the accuracy and stability of the bridge excitation voltage. The bridge output is directly proportional to the excitation voltage, and any drift in the excitation voltage produces a corresponding drift in the output voltage.

For this reason, most all-element varying bridges (such as load cells) are six-lead assemblies: two leads for the bridge output, two leads for the bridge excitation, and two *sense* leads. To take full advantage of the additional accuracy that these extra leads allow, a method called Kelvin or 4-wire sensing is employed, as shown in Figure 4-17.

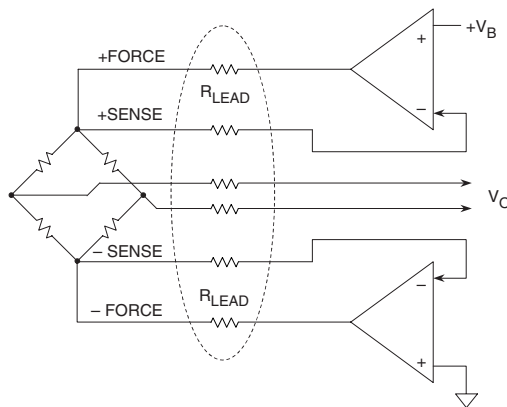


Figure 4-17: A Kelvin sensing system with a 6-wire voltage-driven bridge connection and precision op amps minimizes errors due to wire lead resistances

In this setup the drive voltage V_B is not applied directly to the bridge, but goes instead to the input of the upper precision op amp, which is connected in a feedback loop around the bridge (+) terminal. Although there may be a substantial voltage drop in the +FORCE lead resistance of the remote cable, the op amp will automatically correct for it, since it has a feedback path through the +SENSE lead. The net effect is that the upper node of the remote bridge is maintained at a precise level of V_B (within the capability of the op amp used, of course). A similar situation occurs with the bottom precision op amp, which drives the bridge (-) terminal to a ground level, as established by the op amp input ground reference. Again, the voltage drop in the -FORCE lead is relatively immaterial, because of the sensing at the -SENSE terminal.

In both cases, the sense lines go to high impedance op amp inputs, thus there is minimal error due to the bias current induced voltage drop across their lead resistance. The op amps maintain the required excitation voltage at the remote bridge, to make the voltage measured between the (+) and (-) sense leads always equal to V_B .

Note—a subtle point is that the lower op amp will need to operate on dual supplies, since the drive to the -FORCE lead will cause the op amp output to go negative. Because of relatively high current in the bridge (~30 mA), current buffering stages at the op amp outputs are likely advisable for this circuit.

Although Kelvin sensing eliminates errors due to voltage drops in the bridge wiring resistance, the basic drive voltage V_B must still be highly stable since it directly affects the bridge output voltage. In addition, the op amps must have low offset, low drift, and low noise. Ratiometric operation can be optionally added, simply by using V_B to drive the ADC reference input.

The constant current excitation method shown in Figure 4-18 is another method for minimizing the effects of wiring resistance on the measurement accuracy. This system drives a precise current I through the bridge, proportioned as per the expression in the figure. An advantage of the circuit in Figure 4-18 is that it only uses one amplifier.

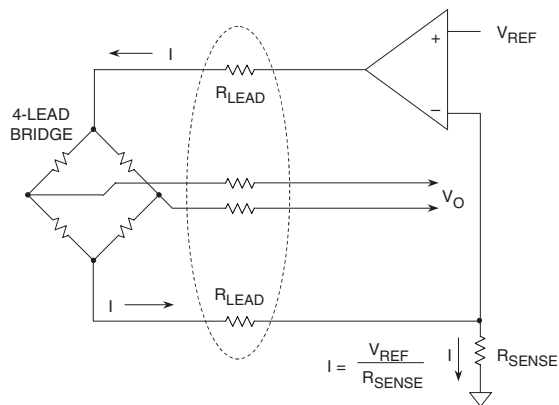


Figure 4-18: A 4-wire current-driven bridge scheme also minimizes errors due to wire lead resistances, plus allows simpler cabling

The accuracy of the reference, the sense resistor, and the op amp all influence the overall accuracy. While the precision required of the op amp should be obvious, one thing not necessarily obvious is that it may be required to deliver appreciable current, when I is more than a few mA (which it will be with standard 350 Ω bridges). In such cases, current buffering of the op amp is again in order.

Therefore for highest precision with this circuit, a buffer stage is recommended. This can be as simple as a small transistor, since the bridge drive is unidirectional.

System Offset Minimization

Maintaining an accuracy of 0.1% or better with a full-scale bridge output voltage of 20 mV requires that the sum of all offset errors be less than 20 μV . Parasitic thermocouples are cases in point and, if not given due attention, can cause serious temperature drift errors. All dissimilar metal-metal connections generate voltages between a few and tens of microvolts for a 1°C temperature differential, are basic thermocouple facts of life.

Fortunately, however, within a bridge measurement system the signal connections are differential; therefore this factor can be used to minimize the impact of parasitic thermocouples.

Figure 4-19 shows some typical sources of offset error that are inevitable in a system. Within a differential signal path, only those thermocouple pairs whose junctions are actually at different temperatures will degrade the signal. The diagram shows a typical parasitic junction formed between the copper printed circuit board traces and the kovar pins of an IC amplifier.

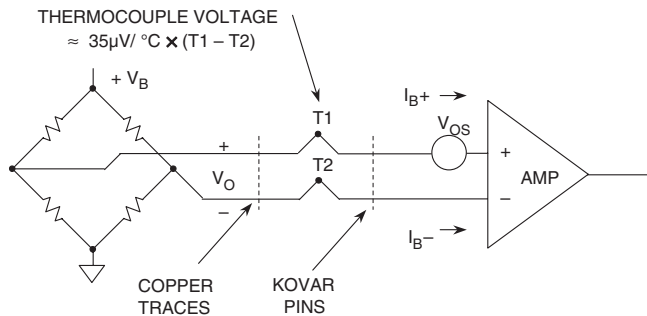


Figure 4-19: Typical sources of offset voltage within bridge measurement systems

This thermocouple voltage is about 35 $\mu\text{V}/^\circ\text{C}$ temperature differential. Note that this package-PC trace thermocouple voltage is significantly less when using a plastic package with a copper lead frame (recommended). Regardless of what package is used, all metal-metal connections along the signal path should be designed so that minimal temperature differences occur between the sides.

The amplifier offset voltage and bias currents are further sources of offset error. The amplifier bias current must flow through the source impedance. Any unbalance in either the source resistances or the bias currents produces offset errors. In addition, the offset voltage and bias currents are a function of temperature.

High performance low offset, low offset drift, low bias current, and low noise precision amplifiers such as the AD707, the OP177 or OP1177 are required. In some cases, chopper-stabilized amplifiers such as the AD8551/AD8552/AD8554 may be a solution. Ac bridge excitation such as that shown in Figure 4-20 can effectively remove offset voltage effects in series with a bridge output, V_O .

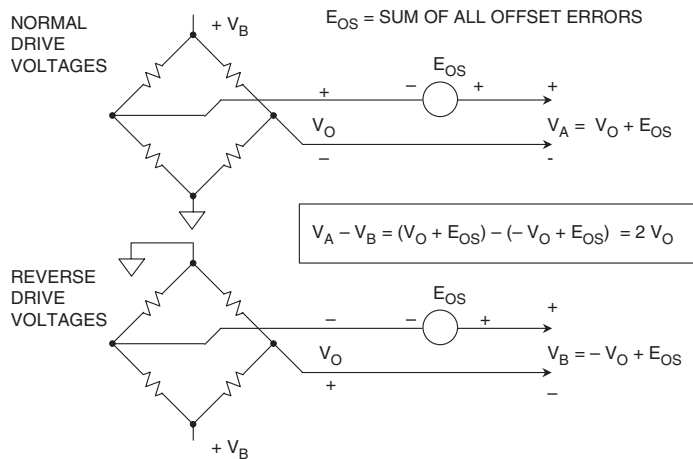


Figure 4-20: Ac bridge excitation minimizes system offset voltages

The concept is simple, and can be described as follows. The net bridge output voltage is measured under the two phased-sequence conditions, as shown. A first measurement (top) drives the bridge at the top node with excitation voltage V_B . This yields a first-phase measurement output V_A , where V_A is the sum of the desired bridge output voltage V_O and the net offset error voltage E_{OS} .

In the second measurement (bottom) the polarity of the bridge excitation is then reversed, and a second measurement, V_B , is made. Subtracting V_B from V_A yields $2V_O$, and the offset error term E_{OS} cancels as noted from the mathematical expression in the figure.

Obviously, a full implementation of this technique requires a highly accurate measurement ADC such as the AD7730 (see Reference 5) as well as a microcontroller to perform the subtraction.

Note that if a ratiometric reference is desired, the ADC must also accommodate the changing polarity of the reference voltage, as well as sense the magnitude. Again, the AD7730 includes this capability.

A very powerful combination of bridge circuit techniques is shown in Figure 4-21, an example of a high performance ADC. In Figure 4-21A is shown a basic dc operated ratiometric technique, combined with Kelvin sensing to minimize errors due to wiring resistance, which eliminates the need for an accurate excitation voltage.

The AD7730 measurement ADC can be driven from a single supply voltage of 5 V, which in this case is also used to excite the remote bridge. Both the analog input and the reference input to the ADC are high impedance and fully differential. By using the + and - SENSE outputs from the bridge as the differential reference voltage to the ADC, there is no loss in measurement accuracy if the actual bridge excitation voltage varies.

To implement ac bridge operation of the AD7730, an “H” bridge driver of P-Channel and N-Channel MOSFETs can be configured as shown in Figure 4-21B (note—dedicated bridge driver chips are available,

References: Bridge Circuits

1. Ramon Pallas-Areny and John G. Webster, **Sensors and Signal Conditioning**, John Wiley, New York, 1991.
2. Dan Sheingold, Editor, **Transducer Interfacing Handbook**, Analog Devices, Inc., 1980, ISBN: 0-916550-05-2.
3. Sections 2, 3, Walt Kester, Editor, **1992 Amplifier Applications Guide**, Analog Devices, 1992, ISBN: 0-916550-10-9.
4. Sections 1, 6, Walt Kester, Editor, **System Applications Guide**, Analog Devices, 1993, ISBN: 0-916550-13-3.
5. Data sheet for **AD7730 Bridge Transducer ADC**, www.analog.com.

Strain, Force, Pressure and Flow Measurements

Walt Kester

Strain Gages

The most popular electrical elements used in force measurements include the resistance strain gage, the semiconductor strain gage, and piezoelectric transducers. The strain gage measures force indirectly by measuring the deflection it produces in a calibrated carrier. Pressure can be converted into a force using an appropriate transducer, and strain gage techniques can then be used to measure pressure. Flow rates can be measured using differential pressure measurements, which also make use of strain gage technology. These principles are summarized in Figure 4-22.

- Strain: Strain Gage, Piezoelectric Transducers
- Force: Load Cell
- Pressure: Diaphragm to Force to Strain Gage
- Flow: Differential Pressure Techniques

Figure 4.22 Strain gages are directly or indirectly the basis for a variety of physical measurements

The resistance-based strain gage uses a resistive element that changes in length, hence resistance, as the force applied to the base on which it is mounted causes stretching or compression. It is perhaps the most well-known transducer for converting force into an electrical variable.

An *unbonded* strain gage consists of a wire stretched between two points. Force acting upon the wire (area = A , length = L , resistivity = ρ) will cause the wire to elongate or shorten, which will cause the resistance to increase or decrease proportionally according to:

$$R = \rho L/A \quad \text{Eq. 4-1}$$

and,

$$\Delta R/R = GF \cdot \Delta L/L \quad \text{Eq. 4-2}$$

where GF = Gage factor (2.0 to 4.5 for metals, and more than 150 for semiconductors).

In this expression, the dimensionless quantity $\Delta L/L$ is a measure of the force applied to the wire and is expressed in *microstrains* ($1 \mu\epsilon = 10^{-6} \text{ cm/cm}$) which is the same as parts-per-million (ppm).

From Eq. 4-2, note that larger gage factors result in proportionally larger resistance changes, hence this implies greater strain gage sensitivity. These concepts are summarized in the drawing of Figure 4-23.

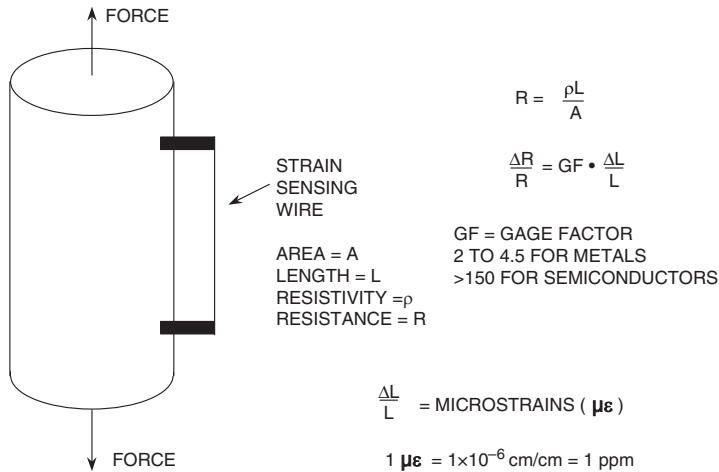


Figure 4-23: Operating principles of a basic unbonded strain gage

A *bonded* strain gage consists of a thin wire or conducting film arranged in a coplanar pattern and cemented to a base or carrier. The basic form of this type of gage is shown in Figure 4-24.

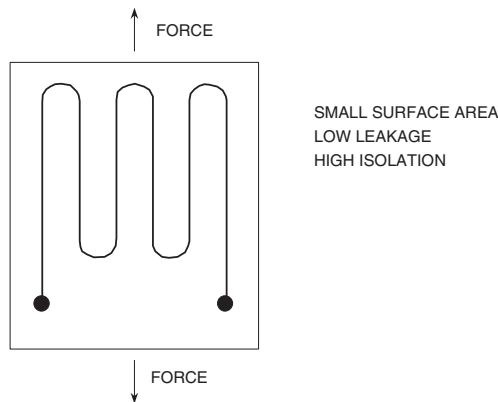


Figure 4-24: A bonded wire strain gage

This strain gage is normally mounted so that as much as possible of the length of the conductor is aligned in the direction of the stress that is being measured, i.e., longitudinally. Lead wires are attached to the base and brought out for interconnection. Bonded devices are considerably more practical and are in much wider use than are the aforementioned unbonded devices.

Perhaps the most popular version is the *foil-type gage*, produced by photo-etching techniques, and using similar metals to the wire types. Typical alloys are of copper-nickel (Constantan), nickel-chromium (Ni-chrome), nickel-iron, platinum-tungsten, and so forth. This strain gage type is shown in Figure 4-25.

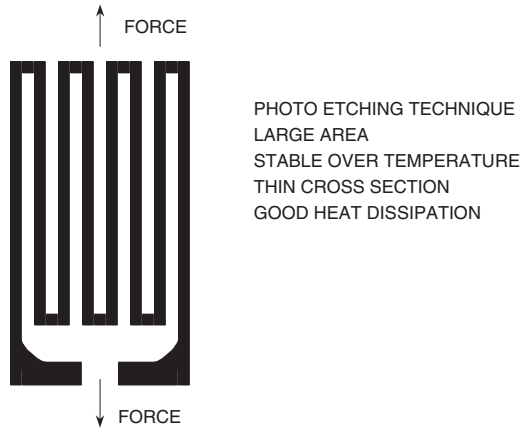


Figure 4-25: A metal foil strain gage

Gages having *wire sensing elements* present a small surface area to the specimen; this reduces leakage currents at high temperatures and permits higher isolation potentials between the sensing element and the specimen. Foil sensing elements, on the other hand, have a large ratio of surface area to cross-sectional area and are more stable under extremes of temperature and prolonged loading. The large surface area and thin cross section also permit the device to follow the specimen temperature and facilitate the dissipation of self-induced heat.

Semiconductor Strain Gages

Semiconductor strain gages make use of the piezoresistive effect in certain semiconductor materials such as silicon and germanium in order to obtain greater sensitivity and higher level output.

Semiconductor gages can be produced to have either positive or negative changes when strained. They can be made physically small while still maintaining a high nominal resistance.

Semiconductor strain gage bridges may have 30 times the sensitivity of bridges employing metal films, but are temperature-sensitive and difficult to compensate. Their change in resistance with strain is also nonlinear. They are not in as widespread use as the more stable metal-film devices for precision work; however, where sensitivity is important and temperature variations are small, they may have some advantage.

Instrumentation is similar to that for metal-film bridges but is less critical because of the higher signal levels and decreased transducer accuracy. Figure 4-26 summarizes the relative performance of metal and semiconductor strain gages.

PARAMETER	METAL STRAIN GAGE	SEMICONDUCTOR STRAIN GAGE
Measurement Range	0.1 to 40,000 $\mu\epsilon$	0.001 to 3000 $\mu\epsilon$
Gage Factor	2.0 to 4.5	50 to 200
Resistance, Ω	120, 350, 600, ..., 5000	1000 to 5000
Resistance Tolerance	0.1% to 0.2%	1% to 2%
Size, mm	0.4 to 150 Standard: 3 to 6	1 to 5

Figure 4-26: A comparison of metal and semiconductor type strain gages

Piezoelectric force transducers are employed where the forces to be measured are dynamic (i.e., continually changing over the period of interest—usually of the order of milliseconds). These devices utilize the effect that changes in charge are produced in certain materials when they are subjected to physical stress. In fact, piezoelectric transducers are *displacement* transducers with quite large charge outputs for very small displacements, but they are invariably used as force transducers on the assumption that in an elastic material, displacement is proportional to force. Piezoelectric devices produce substantial output voltage in instruments such as accelerometers for vibration studies. Piezoelectric sensor output conditioning is discussed within Section 4-4 of this chapter.

Strain gages can be used to measure force, as shown in Figure 4-27, where a cantilever beam is slightly deflected by the applied force. Four strain gages are used to measure the flex of the beam, two on the top, and two on the bottom. The gages are connected in a four-element bridge configuration. Recall from Section 4-2 that this configuration gives maximum sensitivity and is inherently linear. This configuration also offers first-order correction for temperature drift in the individual strain gages.

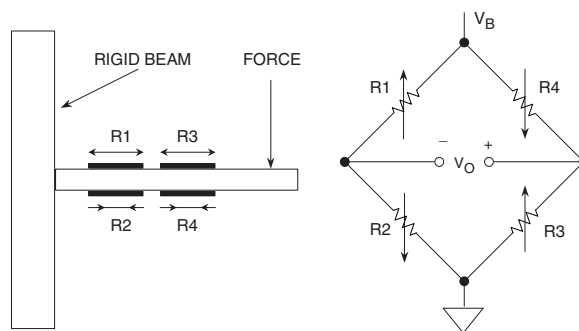


Figure 4-27: A beam force sensor using a strain gage bridge

Strain gages are low-impedance devices, consequently they require significant excitation power to obtain reasonable levels of output voltage. A typical strain-gage-based load cell bridge will have a $350\ \Omega$ impedance and is specified as having a sensitivity in a range $3\ \text{mV}$ – $10\ \text{mV}$ full scale, per volt of excitation.

The load cell is composed of four individual strain gages arranged as a bridge, as shown in Figure 4-28. For a $10\ \text{V}$ bridge excitation voltage with a rating of $3\ \text{mV/V}$, $30\ \text{mV}$ of signal will be available at full-scale loading.

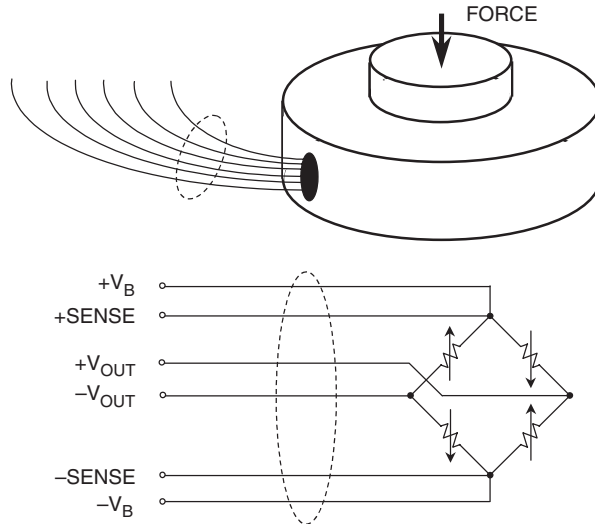


Figure 4-28: A load cell comprising four strain gages is shown in physical (top) and electrical (bottom) representations

While increasing the drive to the bridge can increase the output, self-heating effects are a significant limitation to this approach—they can cause erroneous readings, or even device destruction. One technique for evading this limitation is to use a low duty cycle pulsed drive signal for the excitation.

Many load cells have the \pm “SENSE” connections as shown, to allow the signal-conditioning electronics to compensate for dc drops in the wires (Kelvin sensing as discussed in Section 4-2). This brings the wires to a total of six for the fully instrumented bridge. Some load cells may also have additional internal resistors for temperature compensation purposes.

Pressures in liquids and gases are measured electrically by a variety of pressure transducers. A number of mechanical converters (including diaphragms, capsules, bellows, manometer tubes, and Bourdon tubes) are used to measure pressure by measuring an associated length, distance, or displacement, and to measure pressure changes by the motion produced, as shown by Figure 4-29.

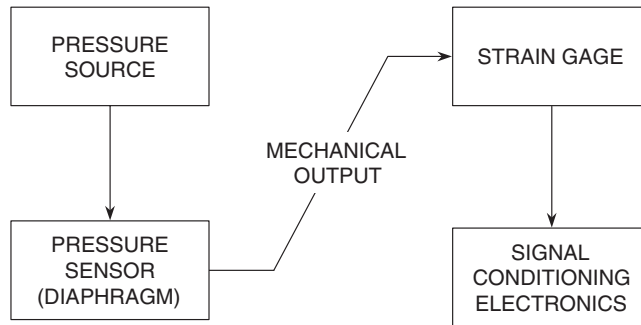


Figure 4-29: Pressure sensors use strain gages for indirect pressure measurement

The output of this mechanical interface is then applied to an electrical converter such as a strain gage, or piezoelectric transducer. Unlike strain gages, piezoelectric pressure transducers are typically used for high frequency pressure measurements (such as sonar applications, or crystal microphones).

There are many ways of defining flow (mass flow, volume flow, laminar flow, turbulent flow). Usually the *amount* of a substance flowing (mass flow) is the most important, and if the fluid's density is constant, a volume flow measurement is a useful substitute that is generally easier to perform. One commonly used class of transducers, which measures flow rate indirectly, involves the measurement of pressure.

Flow can be derived by taking the differential pressure across two points in a flowing medium—one at a static point and one in the flow stream. *Pitot tubes* are one form of device used to perform this function, where flow rate is obtained by measuring the differential pressure with standard pressure transducers.

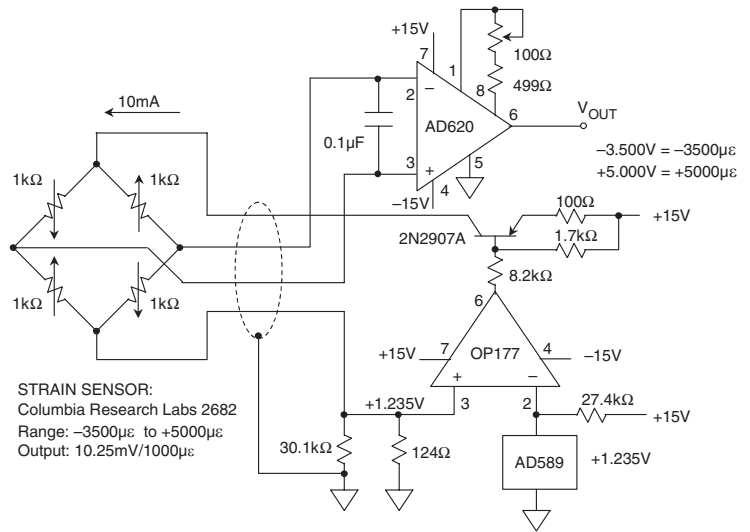
Differential pressure can also be used to measure flow rate using the *venturi* effect by placing a restriction in the flow. Although there are a wide variety of physical parameters being sensed, the electronics interface is very often strain gage based.

Bridge Signal Conditioning Circuits

The remaining discussions of this section deal with applications that apply the bridge and strain gage concepts discussed thus far in general terms.

An example of an all-element varying bridge circuit is a fatigue monitoring strain sensing circuit, as shown in Figure 4-30. The full bridge is an integrated unit, which can be attached to the surface on which the strain or flex is to be measured. In order to facilitate remote sensing, current mode bridge drive is used. The remotely located bridge is connected to the conditioning electronics through a 4-wire shielded cable. The OP177 precision op amp servos the bridge current to 10 mA, being driven from an AD589 reference voltage of 1.235 V. Current buffering of the op amp is employed in the form of the PNP transistor, for lowest op amp self-heating, and highest gain linearity.

Figure 4-30: A precision strain gage sensor amplifier using a remote current-driven 1 kΩ bridge, a buffered precision op amp driver, and a precision in amp 100X gain stage

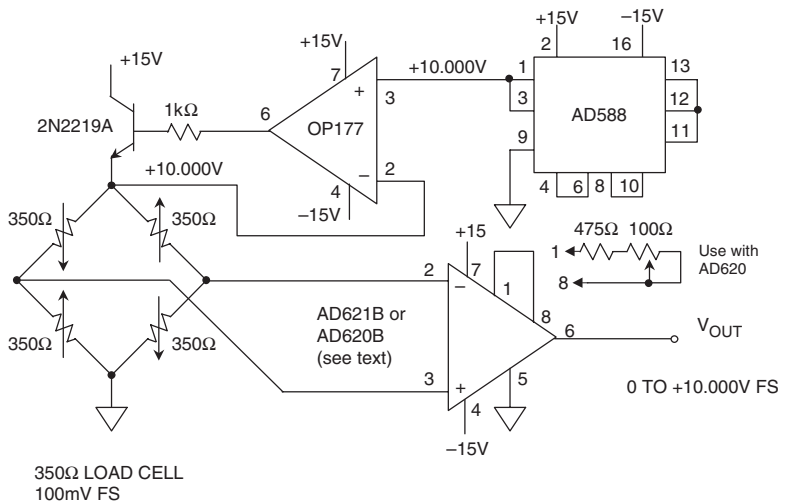


The strain gage produces an output of 10.25 mV/1000 με. The signal is amplified by the AD620 in amp, which is configured for a gain of 100 times, via an effective R_G of 500 Ω. Full-scale voltage calibration is set by adjusting the 100Ω gain potentiometer such that, for a sensor strain of -3500 με, the output reads -3.500 V; and for a strain of +5000 με, the output registers +5.000 V. The measurement may then be digitized with an ADC which has a 10 V full-scale input range.

The 0.1 μF capacitor across the AD620 input pins serves as an EMI/RFI filter in conjunction with the bridge resistance of 1 kΩ. The corner frequency of this filter is approximately 1.6 kHz.

Another example is a load cell amplifier circuit, shown in Figure 4-31. This circuit is more typical of a bridge workhorse application. It interfaces with a typical 350Ω load cell, and can be configured to accommodate typical bridge sensitivities over a range of 3 mV-10 mV/V.

Figure 4-31: A precision 350 Ω load cell amplifier, using a buffered voltage-driven configuration with Kelvin sensing and a precision in amp



A 10.000 V bridge excitation is derived from an AD588 10 V reference, with an OP177 and 2N2219A used as a buffer. The 2N2219A is within the OP177 feedback loop and supplies the necessary bridge drive current (28.57 mA). This ensures that the op amp performance will not be compromised. The Kelvin sensing scheme used at the bridge provides for low errors due to wiring resistances, and a precision zener diode reference, the AD588, provides lowest excitation drift and scaling with temperature changes.

To ensure highest linearity is preserved, a low drift instrumentation amplifier is used as the gain stage. This design has a minimum number of critical resistors and amplifiers, making the entire implementation accurate, stable, and cost effective. In addition to low excitation voltage TC, another stability requirement is minimum in amp gain TC. Both factors are critical towards insuring stable circuit scaling over temperature.

With the use of the AD621B in amp as shown, the scaling is for a precise gain of 100 (as set by the Pin 1–8 jumper), for lowest in amp gain TC. The AD621B is specified for a very low gain TC, only 5 ppm/°C. The gain of 100 translates a 100 mV full-scale bridge output to a nominal 10 V output. Alternately, an AD620B could also be used, with the optional gain network consisting of the fixed 475 Ω resistor, and 100 Ω potentiometer for gain adjustment. This will provide a 50 ppm/°C gain TC for the in amp, plus the TC of the external parts (which should have low temperature coefficients).

While the lowest TC is provided by the fixed gain AD621 setup, it doesn't allow direct control of overall scaling. To retain the very lowest TC, scaling could be accomplished via a software autocalibration routine. Alternately, the AD588 and OP177 reference/op amp stage could be configured for a variable excitation voltage (as opposed to a fixed 10.000 V as shown). Variable gain in the reference voltage driver will effectively alter the excitation voltage as seen by the bridge, and thus provide flexible overall system scaling. Of course, it is imperative that such a scheme be implemented with low TC resistances.

As shown previously, a precision load cell is usually configured as a 350 Ω bridge. Figure 4-32 shows a precision load cell amplifier, within a circuit possessing the advantage of being powered from just a single power supply.

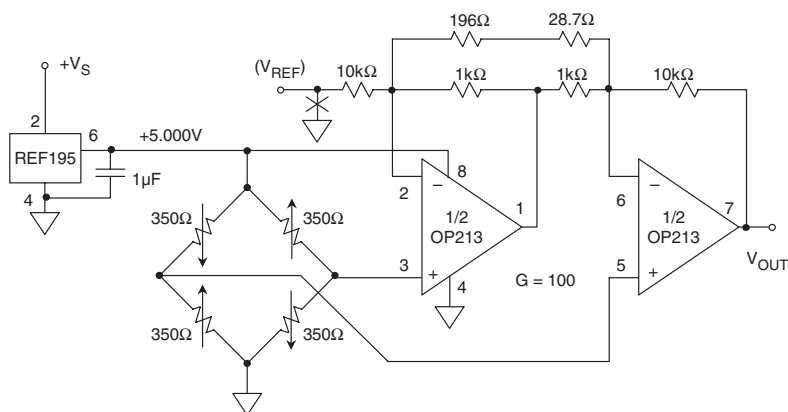


Figure 4-32: a single-supply load cell amplifier

As noted previously, the bridge excitation voltage must be both precise and stable, otherwise it can introduce measurement errors. In this circuit, a precision REF195 5 V reference is used as the bridge drive, allowing a TC as low as 5 ppm/°C. The REF195 reference can also supply more than 30 mA to a load, so

it can drive a 350 Ω bridge (~ 14 mA) without need of a buffer. The dual OP213 is configured as a gain-of-100, two-op-amp in amp. The resistor network sets the gain according to the formula:

$$G = 1 + \frac{10 \text{ k}\Omega}{1 \text{ k}\Omega} + \frac{20 \text{ k}\Omega}{196 \Omega + 28.7 \Omega} = 100 \quad \text{Eq. 4-3}$$

For optimum CMR, the 10 k Ω /1 k Ω resistor ratio matching should be precise. Close tolerance resistors ($\pm 0.5\%$ or better) should be used, and all resistors should be of the same type.

For a zero volt bridge output signal, the amplifier will swing to within 2.5 mV of 0 V. This is the minimum output limit of the OP213. Therefore, if an offset adjustment is required, the adjustment should start from a positive voltage at V_{REF} and adjust V_{REF} downward until the output (V_{OUT}) stops changing. This is the point at which the amplifier limits the swing. Because of the single supply design, the amplifier cannot sense input signals that have negative polarity.

If linearity around or at zero volts input is required, or if negative polarity signals must be processed, the V_{REF} connection can be connected to a stable voltage that is mid-supply (i.e., 2.5 V) rather than ground. Note that when V_{REF} is not at ground, the output must be referenced to V_{REF} . An advantage of this type of referencing is that the output is now bipolar, with respect to V_{REF} .

The AD7730 24-bit sigma-delta ADC is ideal for direct conditioning of bridge outputs, and requires no interface circuitry (see Reference 10). A simplified connection diagram was shown in Figure 4.21A. The entire circuit operates on a single 5 V supply, which also serves as the bridge excitation voltage. Note that the measurement is ratiometric, because the sensed bridge excitation voltage is also used as the ADC reference. Variations in the 5 V supply do not affect the accuracy of the measurement.

The AD7730 has an internal programmable gain amplifier that allows a full-scale bridge output of ± 10 mV to be digitized to 16-bit accuracy. The AD7730 has self- and system calibration features that allow offset and gain errors to be minimized with periodic recalibrations.

A “chop” or ac mode option minimizes the offset voltage and drift and operates similarly to a chopper-stabilized amplifier. The effective input voltage noise RTI is approximately 40 nV rms, or 264 nV peak-to-peak. This corresponds to a resolution of 13 ppm, or approximately 16.5 bits. Gain linearity is also approximately 16 bits.

References: Strain, Force, Pressure And Flow Measurements

1. Ramon Pallas-Areny and John G. Webster, **Sensors and Signal Conditioning**, John Wiley, New York, 1991.
2. Dan Sheingold, Editor, **Transducer Interfacing Handbook**, Analog Devices, Inc., 1980, ISBN: 0-916550-05-2.
3. Sections 2, 3, Walt Kester, Editor, **1992 Amplifier Applications Guide**, Analog Devices, 1992, ISBN: 0-916550-10-9.
4. Sections 1, 6, Walt Kester, Editor, **System Applications Guide**, Analog Devices, 1993, ISBN: 0-916550-13-3.
5. Harry L. Trietley, **Transducers in Mechanical and Electronic Design**, Marcel Dekker, Inc., 1986.
6. Jacob Fraden, **Handbook of Modern Sensors, 2nd Ed.**, Springer-Verlag, New York, NY, 1996.
7. **The Pressure, Strain, and Force Handbook, Vol. 29**, Omega Engineering, One Omega Drive, P.O. Box 4047, Stamford CT, 06907-0047, 1995. www.omega.com.
8. **The Flow and Level Handbook, Vol. 29**, Omega Engineering, One Omega Drive, P.O. Box 4047, Stamford CT, 06907-0047, 1995, www.omega.com.
9. Ernest O. Doebelin, **Measurement Systems Applications and Design, 4th Ed.**, McGraw-Hill, 1990.
10. Data sheet for **AD7730 Bridge Transducer ADC**, www.analog.com.

High Impedance Sensors

Walt Kester, Scott Wurcer, Chuck Kitchin

Many popular sensors have output impedances greater than several megohms, and thus the associated signal-conditioning circuitry must be carefully designed to meet the challenges of low bias current, low noise, and high gain. Figure 4-33 lists a few examples of high impedance sensors.

A large portion of this section is devoted to a germane example, the analysis of a photodiode preamplifier. This application demonstrates many of the problems associated with high impedance sensor signal-conditioning circuits, and offers a host of practical solutions that can be applied to virtually all such sensors.

- Photodiode Preamplifiers
- Piezoelectric Sensors
- Humidity
- pH Monitors
- Chemical Sensors
- Smoke Detectors

Figure 4-33: High impedance sensors

Other examples of high impedance sensors to be discussed are piezoelectric sensors and charge-output sensors.

Photodiode Preamplifier Design

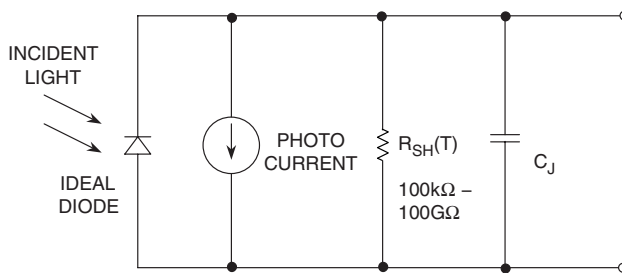
Photodiodes generate a small current that is proportional to the level of illumination. Their applications range from relatively low speed, wide dynamic range circuits to much higher speed circuits. Examples of the types of applications are precision light meters and high-speed fiber optic receivers.

One of the standard methods for specifying photodiode sensitivity is to state its short-circuit photocurrent (I_{sc}) for a given light level from a well-defined light source. The most commonly used source is an incandescent tungsten lamp running at a color temperature of 2850K.

At 100 fc (foot candles) of illumination (approximately the light level on an overcast day), the short-circuit current usually falls in a range of picoamps to hundreds of microamps for small area (less than 1 mm²) diodes.

The equivalent circuit for a photodiode is shown in Figure 4-34. The short-circuit current is very linear over 6 to 9 decades of light intensity, and is therefore often used as a measure of absolute light levels. The open-circuit forward voltage drop across the photodiode varies logarithmically with light level but, because of its large temperature coefficient, the diode voltage is seldom used as an accurate measure of light intensity.

The shunt resistance R_{SH} is usually on the order of $1000\text{ M}\Omega$ at room temperature, and decreases by a factor of 2 for every 10°C rise in temperature. Diode capacitance C_J is a function of junction area and the diode bias voltage. A value of 50 pF at zero bias is typical for small-area diodes.



NOTE: R_{SH} HALVES EVERY 10°C TEMPERATURE RISE

Figure 4-34: A photodiode equivalent circuit

Photodiodes may be operated in either of two basic modes, as shown in Figure 4-35. These modes are with zero bias voltage (*photovoltaic mode*, left) or with a reverse-bias voltage (*photoconductive mode*, right).

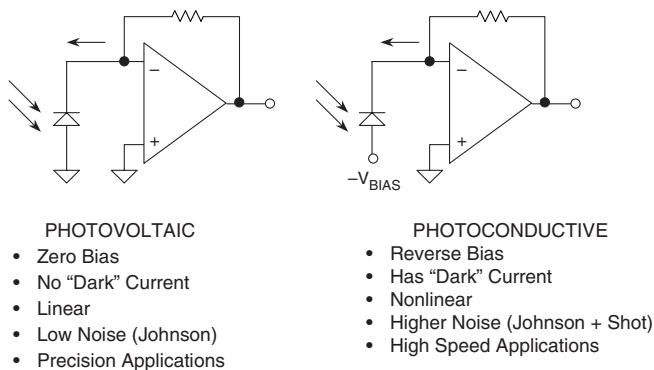


Figure 4-35: Photodiode operating modes

The most precise linear operation is obtained in the photovoltaic mode, while higher switching speeds can be realized when the diode is operated in the photoconductive mode at the expense of linearity. Under these reverse-bias conditions, a small amount of current called *dark current* will flow—even when there is no illumination.

There is no dark current in the photovoltaic mode. In the photovoltaic mode, the diode noise is basically the thermal noise generated by the shunt resistance. In the photoconductive mode, shot noise due to conduction is an additional source of noise. Photodiodes are usually optimized during the design process for use in either the photovoltaic mode or the photoconductive mode, but not both.

Figure 4-36 shows the photosensitivity for a small photodiode (Silicon Detector Part Number SD-020-12-001). This diode has a basic sensitivity of $0.03 \mu\text{A}/\text{fc}$, and was chosen for the design example to follow. As this chart indicates, this photodiode's dynamic range covers six orders of magnitude.

ENVIRONMENT	ILLUMINATION (fc)	SHORT CIRCUIT CURRENT
Direct Sunlight	1000	$30 \mu\text{A}$
Overcast Day	100	$3 \mu\text{A}$
Twilight	1	$0.03 \mu\text{A}$
Full Moonlit Night	0.1	3000pA
Clear Night / No Moon	0.001	30pA

Figure 4-36: Short circuit current versus light intensity for SD-020-12-001 photodiode (photovoltaic operating mode)

A convenient way to convert the photodiode current into a usable voltage is to use a low bias current op amp, configured as a current-to-voltage converter as shown in Figure 4-37. The diode bias is maintained at zero volts by the virtual ground of the op amp, and the short-circuit current is converted into a voltage. At maximum sensitivity the amplifier must be able to detect a diode current of 30 pA . This implies that the feedback resistor must be very large, and the amplifier bias current very small.

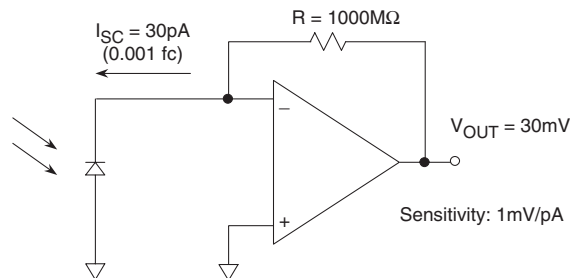


Figure 4-37: A simplified current-to-voltage converter uses a low bias current op amp and a high value feedback resistor

For example, $1000 \text{ M}\Omega$ will yield a corresponding voltage of 30 mV for this amount of current. Larger resistor values are impractical, so we will use $1000 \text{ M}\Omega$ for the most sensitive range. This will give an output voltage range of 10 mV for 10 pA of diode current and 10 V for 10 nA of diode current. This yields a range of 60 dB . For higher values of light intensity, the gain of the circuit must be reduced by using a smaller feedback resistor. For this range of maximum sensitivity, we should be able to easily distinguish between the light intensity on a clear, moonless night (0.001 fc), and that of a full moon (0.1 fc).

Notice that we have chosen to get as much gain as possible from one stage, rather than cascading two stages. This is in order to maximize the signal-to-noise ratio (SNR). If we halve the feedback resistor value, the signal level decreases by a factor of 2, while the noise due to the feedback resistor ($\sqrt{4kTR \cdot \text{Bandwidth}}$) decreases by only $\sqrt{2}$. This reduces the SNR by 3 dB, assuming the closed loop bandwidth remains constant. Later in the analysis, we will find the resistors one of the largest overall output noise contributors.

To accurately measure photodiode currents in the tens of picoamps range, the bias current of the op amp should be no more than a few picoamps. This considerably narrows the choice. The industry-standard OP07 is an ultralow offset voltage (10 μV) bipolar op amp, but its bias current is 4 nA (4000 pA). Even superbeta bipolar op amps with bias current compensation (such as the OP97) have bias currents on the order of 100 pA at room temperature, but they might be suitable for very high temperature applications, as unlike FET amplifiers, the bias currents do not double for every 10°C increase.

A JFET input electrometer-grade op amp is chosen for our photodiode preamp, since it must operate only over a limited temperature range. Figure 4-38 summarizes the performance of several popular “electrometer grade” FET input op amps.

PART #	$V_{OS, \text{MAX}}^*$	$TC V_{OS, \text{TYP}}$	$I_{B, \text{MAX}}^*$	0.1Hz TO 10Hz NOISE, TYP	PACKAGE
AD549K	250 μV	5 $\mu\text{V}/^\circ\text{C}$	100fA	4 μV p-p	TO-99
AD795JR	500 μV	3 $\mu\text{V}/^\circ\text{C}$	3pA	1 μV p-p	SOIC
AD820B	1000 μV	2 $\mu\text{V}/^\circ\text{C}$	10pA	2 μV p-p	SOIC, DIP

*25°C SPECIFICATION

Figure 4-38: Some JFET input electrometer grade op amps suitable for use in photodiode preamplifiers

As can be noted from this figure, the 25°C maximum bias current specification ranges from a few pA down to as low as 100 fA, and there are a number of packages types from which to choose. As will be seen shortly, the package finally chosen can and will affect the performance of the circuit in terms of the bias current realized within an application. This is due to relative ability to control the inevitable leakage currents in a design’s production environment.

Of these devices, the AD549 and AD795 are fabricated on a BiFET process and use P-Channel JFETs as the input stage, as is shown in Figure 4-39. The rest of the op amp circuit is designed using bipolar devices. These BiFET op amps are laser trimmed at the wafer level, to minimize offset voltage and offset voltage drift. The offset voltage drift is minimized, by first trimming the input stage for equal currents in the JFET differential pair (drift trim resistors). A further trim of the JFET source resistors minimizes the input offset voltage (offset voltage trim resistors).

For these discussions, an AD795JR was selected for the photodiode preamplifier, with key specifications summarized in Figure 4-38. This allows high circuit performance in an SOIC packaged device.

Alternately, for even greater performance, the AD549 could be used. The AD549 uses the glass sealed TO-99 package, which allows the very highest performance in terms of low leakage. More on this follows.

Since the photodiode current is measured in terms of picoamperes, it should be understood that extremely close attention must be given to all potential leakage paths in the actual physical circuit. To put this in some

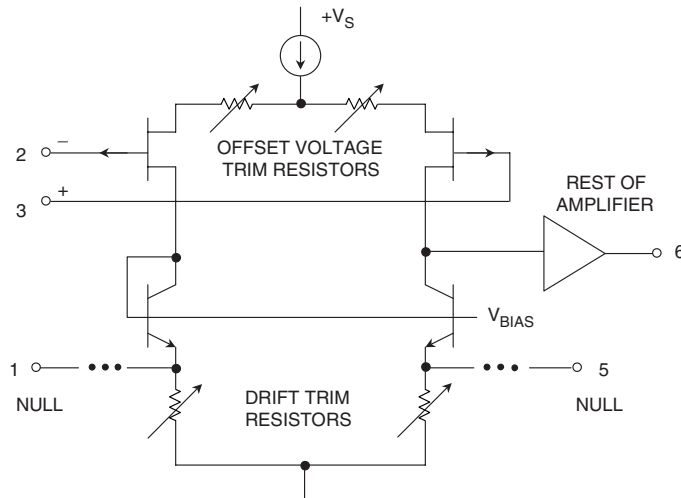


Figure 4-39: JFET input stage op amp with separate trims for offset voltage and drift

perspective, consider the a simple printed circuit card example with two parallel conductor traces on a high-quality, well-cleaned epoxy-glass PC board 0.05 inches apart and parallel for 1 inch. Such an insulator has a leakage resistance of approximately $10^{11} \Omega$ at $+125^\circ\text{C}$. By simple application of Ohm's law, 15 V of bias between these runs produces a 150 pA current—sufficient to mask all signal levels below this current. Obviously then, low-level photodiode circuitry needs to employ all possible means of minimizing such parasitic currents. Unfortunately, they can arise from numerous sources, some of which can be quite subtle in origin.

Figure 4-40 illustrates the circuit elements subject to leakage for the photodiode circuit, as enclosed within the dotted lines. The feedback resistor is highly critical, and should be a close tolerance (1%), low TC (50 ppm/ $^\circ\text{C}$) unit. Typical units suitable for R2 will be manufactured with thin film or metal oxide construction on ceramic or glass, with glass insulation. It should be readily apparent that any shunt conductive paths

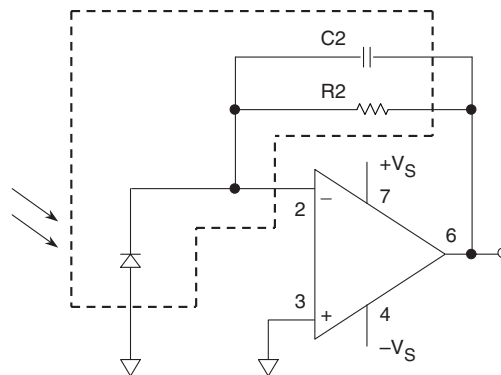


Figure 4-40: Critical leakage paths and components for a photodiode preamplifier circuit are those within the dotted line area

across this resistor's body can (and will) degrade or lower the net effective resistance, producing scaling errors. It is for this reason that such high value resistors are often glass enclosed, and can require special handling. Some sources of suitable high value resistors are listed in the section references. If used, compensation capacitor C2 should use the lowest loss dielectric possible. Typically this will mean a film type capacitor of Teflon, polypropylene, or polystyrene construction.

All connections to the op amp's summing junction should be kept short, clean, and free from manufacturing process chemicals and residues. In cases where an input cable is used to connect the photodiode to the pre-amp, it should be kept as short as possible, and should use Teflon or similar low loss dielectric insulation.

The above considerations deal mainly with the more obvious construction points towards optimizing accuracy and keeping leakage low. However, two of the more difficult leakage sources that can plague this circuit aren't quite as obvious. These are the op amp package-related parasitic leakages, which can occur from all op amp package pins adjacent to the input pin. Consider leakage as a high value resistance to Pin 2.

Although it doesn't show in this particular figure (since Pin 1 isn't actively used by the application), *any leakage from package Pin 1 can be very relevant*. Note also, that since Pin 3 is grounded, it prevents error from leakage between Pins 4 and 2. If however, Pin 1 has any significant voltage on it (which it does in the case of the offset null pin of the AD820BN DIP device) serious leakage will then occur between Pins 1 and 2. The AD795JR SOIC is immune to this leakage, as Pin 1 isn't connected internally. These comments serve to illustrate some of the subtleties of these leakage sources.

The situation just described for the AD820BN DIP packaged device is by no means unique, as Pin 1 is a standard offset trim pin on many op amps. This circumstance will always tend to leak current into any high impedance source seen at Pin 2. There are also cases for follower-connected stages where leakage is just as critical, if not more so. In such cases the leakage goes into Pin 3 as a high impedance, typically from Pin 4, which is $-V_s$. Fortunately however, there is a highly effective answer to controlling both of these leakage problems, and that is the use of circuit *guard* techniques.

Guarding is used to reduce parasitic leakage currents, by isolating a sensitive amplifier input from large voltage gradients across the PC board. It does this by interposing a conductive barrier or screen between a high voltage source and a sensitive input. The barrier intercepts the leakage which would otherwise flow into the sensitive node, and diverts it away. In physical terms, a guard is a low impedance conductor that completely surrounds an input line or node, and it is biased to a potential equal to the line's voltage.

Note that the low impedance nature of a guard conductor shunts leakage harmlessly away. The biasing of the guard to the same potential as the guarded pin reduces any possibility of leakage between the guard itself and the guarded node. The exact technique for guarding depends on the amplifier's mode of operation, i.e., whether the connection is inverting (like Figure 4-40), or a noninverting stage.

Figure 4-41 shows a PC board layout for guarding the inputs of the AD820 op amp, as operated within either an inverting (top) or a noninverting gain stage (bottom). This setup uses the DIP ("N") package, and would also be applicable to other devices where relatively high voltages occur at Pin 1 or 4. Using a standard 8-pin DIP outline, it can be noted that this package's 0.1" pin spacing allows a PC trace (the guard trace) to pass between adjacent pins. This is the key to implementing effective DIP package guarding—the complete surrounding of the guarded trace with a low impedance trace.

In the inverting mode (top), note that Pin 3 connected and grounded guard traces surround the op amp inverting input (Pin 2), and run parallel to the input trace. This guard would be continued out to and around the source device and feedback connection in the case of a photodiode (or around the input pad, in the case of a cable). In the follower mode (bottom), the guard voltage is the feedback divider tap voltage to Pin 2, i.e., the inverting input node of the amplifier. Although the feedback divider impedance isn't as low

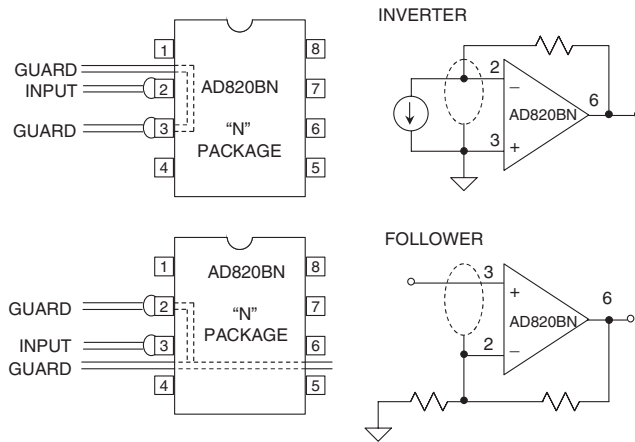


Figure 4-41: Guard techniques for inverting and noninverting op amp stages using DIP package devices

in absolute terms as a direct ground, it is still quite effective. Even a 1 k Ω or so impedance here will still be many orders of magnitude lower than the Pin 3 impedance. In both the inverting and the noninverting modes, the guard traces should be located on both sides of the PC board, with top and bottom side traces connected with several vias. Things become slightly more complicated when using guarding techniques with the SOIC surface mount (“R”) package, because the 0.05" pin spacing doesn't allow routing of PC board traces between the pins. But there still is an effective guarding answer, at least for the inverting case. Figure 4-42 shows the preferred method.

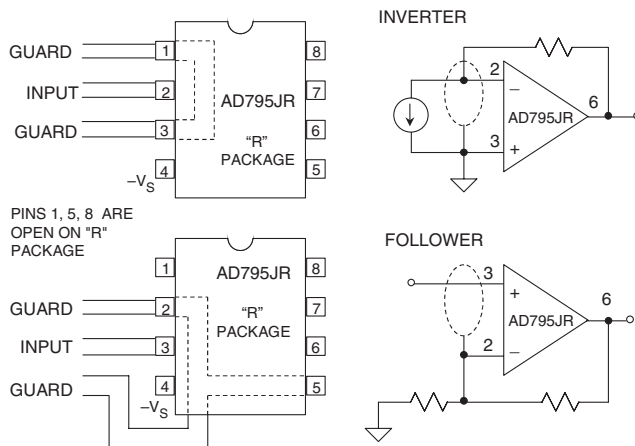


Figure 4-42: Guard techniques for inverting and noninverting op amp stages using SOIC package devices

In the AD795 SOIC “R” package, Pins 1, 5, and 8 are “no-connect” pins and can be used to route signal traces as shown. Thus in the case of the inverting stage (top), guarding is still completely effective, with dummy Pin 1 and Pin 3 acting as a grounded guard trace.

In the case of the follower stage (bottom), the guard trace must be routed around the $-V_S$ pin, and thus the Pin 4 to Pin 3 leakage is *not* fully guarded. For this reason, a very high impedance follower stage using an SOIC package op amp isn’t generally recommended, as adequate guarding simply isn’t possible. An exception to this caveat would apply the use of a *single-supply* op amp as a follower (for example, the AD820), in which case Pin 4 becomes grounded by default, and some degree of intrinsic guarding is established.

For extremely low bias current applications, such as for example with the AD549 with input bias current of 100 fA, the high impedance input signal connection of the op amp should be made to a virgin Teflon stand-off insulator, as shown in Figure 4-43. Note—“virgin” Teflon is a solid piece of new Teflon material that has been machined to shape (as opposed to one welded together from powder or grains).

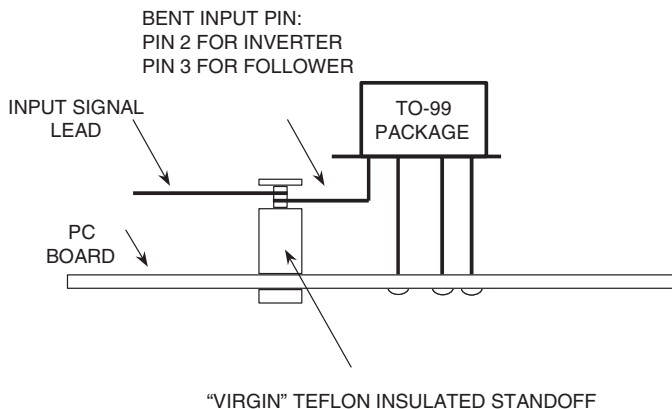


Figure 4-43: Input pin isolation technique using virgin Teflon standoff insulator

If mechanical and manufacturing considerations allow, the sensitive op amp input pin should be soldered directly to the Teflon standoff, rather than going through a PCB hole.

For TO-99 packaged devices, such as the AD549KH, two possible guarding choices present themselves. One method is to employ the device in a scheme like Figure 4-43, with the sensitive input pin going to the Teflon stand-off. Alternately, a round PCB layout scheme that is more amenable to the TO-99 package can be used, as shown in Figure 4-44.

This scheme uses a guard ring, which completely surrounds the input and feedback nodes, with the ring tied to the device’s metal can through the Pin 8 connection. The guard ring is then also tied to either ground or the feedback divider, as suits the application. This setup can also be further modified, to use the more sensitive of the two inputs going to a *Teflon stand-off within the guard ring*, for the ultimate in performance.

Note that in all cases where control of leakage is critical, the PC board itself must be carefully cleaned and then sealed against humidity and dirt using a high quality conformal coating material. In addition to minimizing leakage currents, the entire circuit should be well shielded with a grounded metal shield to prevent stray signal pickup.

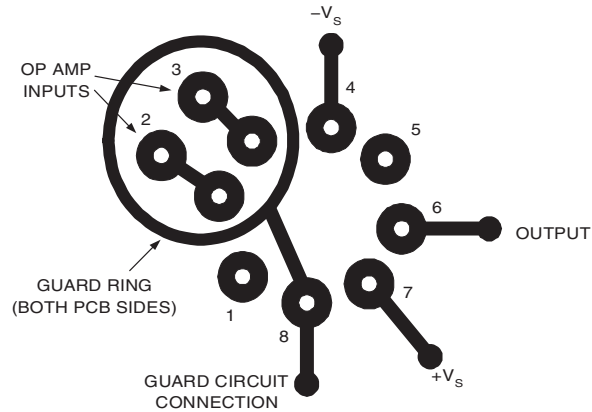
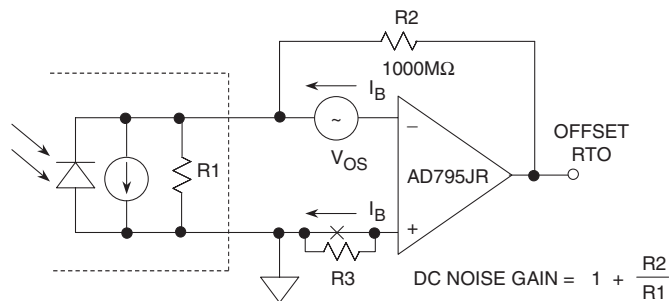


Figure 4-44: TO-99 package devices can use guard rings surrounding input pins 2 and 3 (PCB bottom view shown)

Preamplifier Offset Voltage and Drift Analysis

A photodiode preamp offset voltage and bias current model is shown in Figure 4-45. There are two important considerations in this circuit. First, the diode shunt resistance (R_1) is a function of temperature—it halves every time the temperature increases by 10°C . At room temperature (25°C), $R_1 = 1000\ \text{M}\Omega$, but at 70°C it decreases to $43\ \text{M}\Omega$. This has a drastic impact on the circuit noise gain and hence the output offset voltage. In the example, at 25°C the dc noise gain is 2, but at 70°C it increases to 24.

The second circuit difficulty is that the input bias current doubles with every 10°C temperature rise. The bias current produces an output offset error equal to $I_B R_2$. At 70°C bias current increases to $72\ \text{pA}$, compared to $3\ \text{pA}$ at room temperature. Normally, the addition of a resistor (R_3) between the noninverting input of the op amp and ground, with a value of $R_1 \parallel R_2$ would yield a first-order cancellation of this effect. However, because R_1 changes with temperature, this method simply isn't effective. In addition, if R_3 is



- I_B DOUBLES EVERY 10°C TEMPERATURE RISE
- $R_1 = 1000\text{M}\Omega$ @ 25°C (DIODE SHUNT RESISTANCE)
- R_1 HALVES EVERY 10°C TEMPERATURE RISE
- R_3 CANCELLATION RESISTOR NOT EFFECTIVE

Figure 4-45: AD795JR photodiode preamplifier offset error model

used, the bias current then develops a voltage across it, which in turn would be applied to the photodiode as a parasitic bias. Such a bias would cause the diode response to become nonlinear, thus the use of R3 is also undesirable from a linearity point-of-view.

The total referred-to-output (RTO) offset voltage preamp errors are summarized in Figure 4-46. Notice that at 70°C the total error is 87.2 mV. This error is acceptable for the design under consideration. The primary contributor to the error at high temperature is of course the bias current.

	0°C	25°C	50°C	70°C
V_{OS}	0.575mV	0.500mV	0.575mV	0.635mV
Noise Gain	1.1	2	7	24
V_{OS} Error RTO	0.6mV	1.0mV	4.0mV	15.2mV
I_B	0.6pA	3.0pA	18.0pA	72.0pA
I_B Error RTO	0.6mV	3.0mV	18.0mV	72.0mV
Total Error RTO	1.2mV	4.0mV	22.0mV	87.2mV

Figure 4-46: AD795JR photodiode preamplifier offset error summary

Several steps can be taken to minimize amplifier temperature rise, and thus offset drift. Operating the amplifier at reduced supply voltages, minimizing the output drive requirements, and heat sinking are some ways to reduce this error. The addition of an external offset nulling circuit would minimize the initial input offset voltage error.

Thermoelectric Voltages as Sources of Input Offset Voltage

As discussed earlier in this chapter, thermoelectric potentials are generated by electrical connections are made between different metals. For example, the copper PC board electrical contacts to the kovar input pins of a TO-99 IC package can create an offset voltage of up to 40 $\mu\text{V}/^\circ\text{C}$, if the two bimetal junctions so formed are at different temperatures. Even ordinary solders, being composed of alloys different from PCB copper traces, can give rise to thermoelectric voltages. For example, common high tin content lead-tin solder alloys, when used with copper, create thermoelectric voltages on the order of 1 $\mu\text{V}/^\circ\text{C}$ to 3 $\mu\text{V}/^\circ\text{C}$ (see Reference 8). While some special cadmium-tin solders can reduce this voltage to 0.3 $\mu\text{V}/^\circ\text{C}$, cadmium solders aren't in general use for health reasons. Another possible low thermal EMF solder is a low tin alloy such as Sn10Pb90.

The best general solution to minimizing this spurious thermocouple problem is to ensure that the connections to the inverting and noninverting input pins of the IC are made with the same material, and that the PC board thermal layout is such that these two pins remain at the same temperature. Everything should be balanced from a thermal standpoint. In the case where a Teflon standoff is used as an insulated connection point for the inverting input (as in the case of this preamp), prudence dictates that connections to the noninverting inputs also be made in a similar manner to minimize possible thermoelectric effects, and in keeping with the principle of thermal symmetry.

Preamplifier AC Design, Bandwidth, and Stability

The key to the preamplifier ac design is an understanding of the circuit noise gain as a function of frequency. Plotting gain versus frequency on a log-log scale makes the analysis relatively simple (see Figure 4-47). This type of plot is also referred to as a Bode plot. The noise gain is the gain seen by a small voltage source in series with one of the op amp input terminals. It is also the same as the noninverting signal gain (the gain from “A” to the output). In the photodiode preamplifier, the signal current from the photodiode passes through the C2/R2 network. It is important to distinguish between the signal gain and the noise gain, because it is the noise gain characteristic that determines the net circuit stability, regardless of where the signal is actually applied.

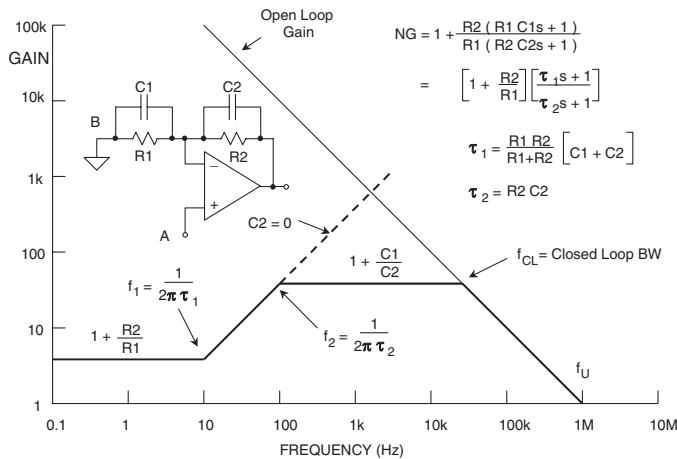


Figure 4-47: A generalized noise gain Bode plot

Note that the net slope between the noise gain and the open loop gain curves, *at the point where they intersect*, determines system stability. For unconditional stability, the noise gain curve must intersect the open loop response with a net slope of less than 12 dB/octave (or 20 dB per decade). In the figure, the dotted ($C2 = 0$) line shows a noise gain that intersects the open loop gain at a net slope of 12 dB/octave, indicating an unstable condition. This is what would occur in the circuit, without a feedback capacitor.

The general equations for determining the break points and gain values in the Bode plot are also given in Figure 4-47. It is useful to examine these gain characteristics with increasing frequency. At low frequencies, the circuit noise gain is $1 + R2/R1$, as indicated by the lowest frequency shelf (below 10 Hz). There are two key time constants in this circuit, τ_1 and τ_2 . The first comes into play as a zero in the noise gain transfer function, which occurs at a frequency of $f_1 = 1/2\pi\tau_1$, where $\tau_1 = R1 \parallel R2 (C1 + C2)$. Stated simply, this frequency falls where the noise gain begins to increase to a new (higher) value from the low frequency gain of $1 + R2/R1$ plateau. In the Figure 4-47 example f_1 occurs at 10 Hz.

Above f_1 , gain increases towards a high frequency gain plateau where the gain is $1 + C1/C2$, which is indicated as the highest frequency shelf (above 100 Hz). The second time constant, τ_2 , comes into play as a pole of the transfer function, which occurs at a corner frequency, $f_2 = 1/2\pi\tau_2$, where $\tau_2 = R2C2$. It can also be noted that this is equal to the signal bandwidth, if the signal is applied at point “B.”

Plotting the composite noise gain curve on the log-log graph is a simple matter of connecting the f_1 and f_2 breakpoints with a line having a 45° slope, after first sketching the flat low and high frequency gain plateaus. The point at which the high frequency noise gain intersects the op amp open loop gain is called the *closed loop bandwidth*. Notice that the *signal bandwidth* for a signal applied at point “B” is much less, and is $1/2 \pi R_2 C_2$.

Figure 4-48 shows the noise gain plot for the photodiode preamplifier using actual circuit values. The choice of C2 determines the actual signal bandwidth and also the phase margin. In the example, a signal bandwidth of 16 Hz was chosen. Notice that a smaller value of C2 would result in a higher signal bandwidth and a corresponding reduction in phase margin. It is also interesting to note that although the signal bandwidth is only 16 Hz, the closed loop bandwidth is 167 kHz. This will have important implications with respect to the output noise voltage analysis to follow.

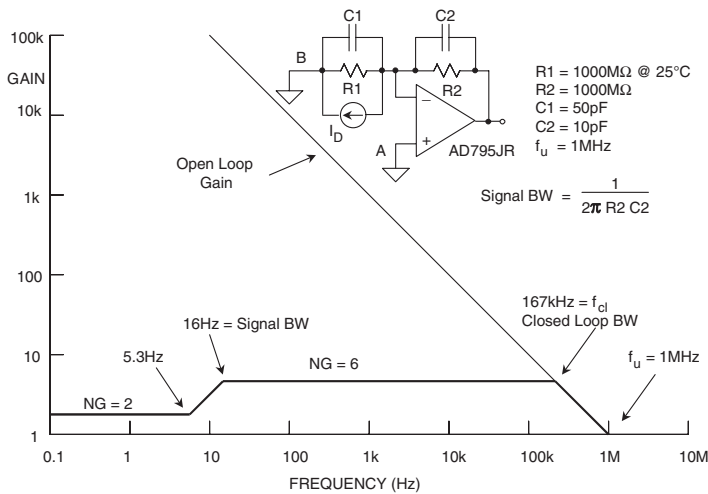


Figure 4-48: Noise gain of the AD795 photodiode preamplifier at 25°C

It is important to note that temperature changes do not significantly affect the stability of the circuit. Changes in R1 (the photodiode shunt resistance) affect only the low frequency noise gain and the frequency at which the zero in the noise gain response occurs. The high frequency noise gain is determined by the C1/C2 ratio.

Photodiode Preamplifier Noise Analysis

To begin a noise analysis, we first consider the AD795 input voltage and current noise spectral densities, as shown in Figure 4-49. The AD795 performance is truly impressive for a JFET input op amp: 1 μ V p-p typical 0.1 Hz to 10 Hz noise, and a 1/f corner frequency of 12 Hz, comparing favorably with all but the best bipolar op amps. As shown in the (right) figure, the current noise is much lower than for bipolar op amps, a key factor making it an ideal choice for high impedance applications.

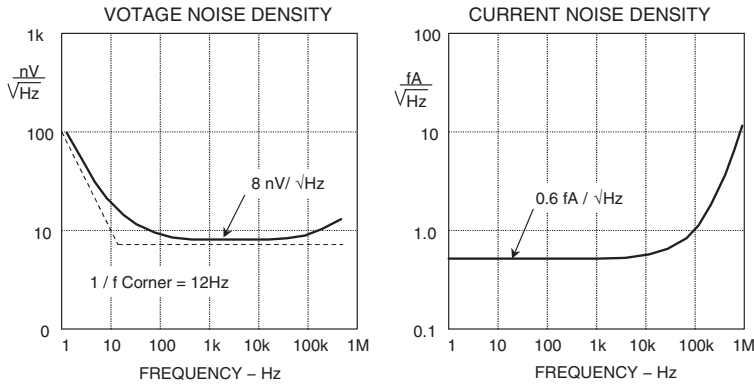


Figure 4-49: AD795 Voltage and current noise density performance

The complete noise model for an op amp is shown in Figure 4-50. This model includes the reactive elements C1 and C2. Each individual output noise contributor is calculated by integrating the square of its spectral density over the appropriate frequency bandwidth and then taking the square root, as:

$$\text{RMS OUTPUT NOISE DUE TO } V_1 = \sqrt{\int V_1(f)^2 df} \quad \text{Eq. 4-4}$$

In most cases, this integration can be done by inspection of the graph of the individual spectral densities superimposed on a graph of the noise gain. The total output noise is then obtained by combining the individual components in a root-sum-squares manner. The table in the diagram shows how each individual source is reflected to the output, and the corresponding bandwidth for integration. The factor of 1.57 ($\pi/2$) is required to convert the single-pole bandwidth into its equivalent noise bandwidth.

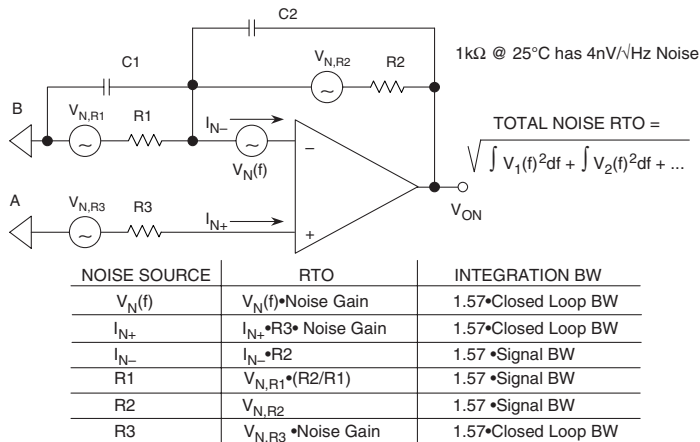


Figure 4-50: A noise model of preamp

The resistor Johnson noise spectral density V_R is given by:

$$V_R = \sqrt{4kTR} \quad \text{Eq. 4-5}$$

where R is the resistance in ohms, k is Boltzmann's constant (1.38×10^{-23} J/K), and T is the absolute temperature in Kelvins.

A simple way to compute this is to remember that the noise spectral density of a 1 k Ω resistor is 4 nV/ $\sqrt{\text{Hz}}$ at +25°C. The Johnson noise of another resistor value can be found by multiplying by the square root of the ratio of the resistor value to 1000 Ω . For example, a 4 k Ω resistor produces a noise density $\sqrt{4}$ times a 1 k Ω resistor, or 8 nV/ $\sqrt{\text{Hz}}$ (at +25°C).

Finally, note that Johnson noise is broadband, and its spectral density is constant with frequency.

Input Voltage Noise

In order to obtain the output voltage noise spectral density plot due to the input voltage noise, the input voltage noise spectral density plot is multiplied by the noise gain plot. This is easily accomplished using the Bode plot on a log-log scale. The total RMS output voltage noise due to the input voltage noise is then obtained by integrating the square of the output voltage noise spectral density plot, and then taking the square root. In most cases, this integration may be approximated. A lower frequency limit of 0.01 Hz in the 1/f region is normally used. If the bandwidth of integration for the input voltage noise is greater than a few hundred Hz, the input voltage noise spectral density may be assumed to be constant. Usually, the value of the input voltage noise spectral density at 1 kHz will provide sufficient accuracy.

It is important to note that the input voltage noise contribution must be integrated over the entire closed-loop bandwidth of the circuit (the closed loop bandwidth, f_{cl} , is the frequency at which the noise gain intersects the op amp open loop response). This is also true of the other noise contributors that are reflected to the output by the noise gain (namely, the non inverting input current noise and the non inverting input resistor noise).

The inverting input noise current flows through the feedback network to produce a noise voltage contribution at the output. The input noise current is approximately constant with frequency, therefore, the integration is accomplished by multiplying the noise current spectral density (measured at 1 kHz) by the noise bandwidth which is 1.57 times the signal bandwidth ($1/2 \pi R_2 C_2$). The factor of 1.57 ($\pi/2$) arises when single-pole 3 dB bandwidth is converted to equivalent noise bandwidth.

Johnson Noise Due to Feedforward Resistor R1

The noise current produced by the feedforward resistor R1 also flows through the feedback network to produce a contribution at the output. The noise bandwidth for integration is also 1.57 times the signal bandwidth.

Noninverting Input Current Noise

The noninverting input current noise, I_{N+} , develops a voltage noise across R3 that is reflected to the output by the noise gain of the circuit. The bandwidth for integration is therefore the closed-loop bandwidth of the circuit. However, there is no contribution at the output if R3 = 0 (or, if R3 is used, but it is bypassed with a large capacitor). This will usually be desirable when operating the op amp in the inverting mode.

Johnson Noise Due to Resistor in Noninverting Input

The Johnson voltage noise due to R3 is also reflected to the output by the noise gain of the circuit. Again, if R3 is bypassed sufficiently, it makes no significant contribution to the output noise.

Summary of Photodiode Circuit Noise Performance

Figure 4-51 shows the output noise spectral densities for each of the contributors at 25°C. As can be noted, there is no contribution due to I_{N+} or R3, since the noninverting input of the op amp is grounded.

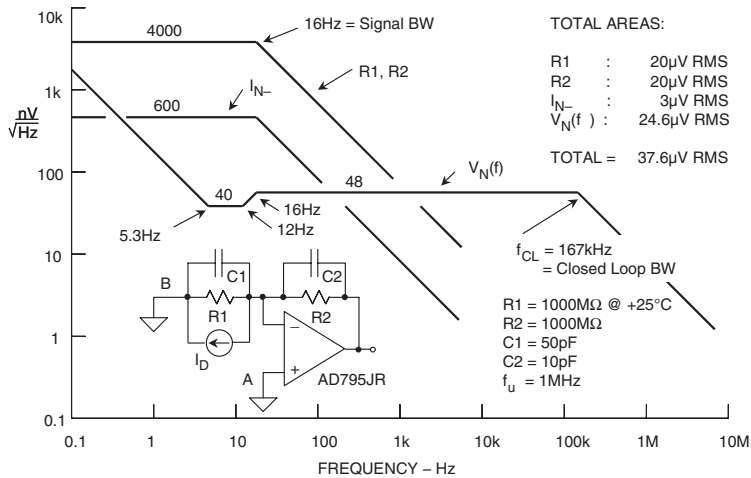


Figure 4-51: Preamp output spectral noise densities (nV/\sqrt{Hz}) @25°C

Noise Reduction Using Output Filtering

From the above analysis, the largest contributor to the output noise voltage at 25°C is the input voltage noise of the op amp reflected to the output by the noise gain. This contributor is large primarily because the noise gain over which the integration is performed extends to a bandwidth of 167 kHz (the intersection of the noise gain curve with the open-loop response of the op amp). If the op amp output is filtered by a single-pole low-pass filter with a 20 Hz cutoff frequency ($\tau = 7.95$ ms), this contribution is reduced to less than 1 μVrms . The diagram for the final, filtered, optimized photodiode circuit design is shown in Figure 4-52.

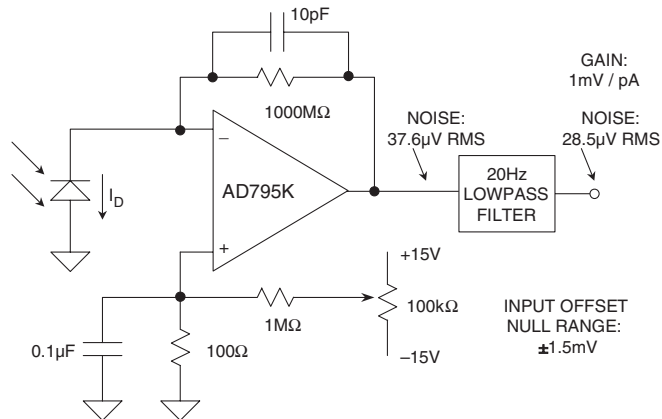


Figure 4-52: AD795K preamp with output filter and offset null option

Notice that the same results would not be achieved simply by increasing the feedback capacitor, C_2 . Increasing C_2 lowers the high frequency noise gain, but the integration bandwidth becomes proportionally higher. Larger values of C_2 may also decrease the signal bandwidth to unacceptable levels.

The addition of the post-filter stage reduces output noise to 28.5 μVrms ; approximately 75% of its former value, and the resistor noise and current noise are now the largest contributors to output noise. Practically, this filter can be either active or passive. Care will need to be taken, of course, that the filter circuit does not add any significant noise of its own to the signal. Filter design is discussed in greater detail in Chapter 5 of this book. The final circuit also includes an offset trim arrangement that is capable of nulling op amp offsets of up to ± 1.5 mV.

Summary of Circuit Performance

Performance characteristics are summarized in Figure 4-53. The total output voltage drift over 0 to 70°C is 87.2 mV, corresponding to 87.2 pA of diode current. The offset nulling circuit shown on the noninverting input can be used to null out the room temperature offset. Note that this method is better than using the offset null pins because using the offset null pins will increase the offset voltage TC by about 3 $\mu\text{V}/^\circ\text{C}$ for each millivolt nulled. In addition, the AD795 SOIC package does not have offset nulling pins.

The input sensitivity based on a total output voltage noise of 44 μV is obtained by dividing the output voltage noise by the value of the feedback resistor R_2 . This yields a minimum detectable diode current of 44 fA. If a 12-bit ADC is used to digitize the 10 V full-scale output, the weight of the least significant bit (LSB) is 2.5 mV. The output noise level is much less than this.

- Output Offset Error (0°C to 70°C) : 87.2mV
- Output Sensitivity: 1mV/pA
- Output Photosensitivity: 30V / foot-candle
- Total Output Noise @ 25°C : 28.5µV RMS
- Total Noise RT1 @ 25°C : 44fA RMS, or 26.4pA p-p
- Range with R2 = 1000MΩ: 0.001 to 0.33 foot-candles
- Bandwidth: 16Hz

Figure 4-53: AD795JR photodiode preamp performance summary

Photodiode Circuit Trade-off

Many trade-offs could be made in the basic photodiode circuit design we have described. More signal bandwidth can be achieved in exchange for a larger output noise level. Reducing the feedback capacitor C2 to 1 pF increases the signal bandwidth to approximately 160 Hz. Further reductions in C2 are not practical because the parasitic capacitance is probably in the order of 1 pF to 2 pF. Some small amount of feedback capacitance is also required to maintain stability.

If the circuit is to be operated at higher levels of illumination (greater than approximately 0.3 fc), the value of the feedback resistor can be reduced, thereby resulting in further increases in circuit bandwidth and less resistor noise.

If gain-ranging is to be used to measure higher light levels, extreme care must be taken in the design and layout of the additional switching networks to minimize leakage paths and other parasitic effects.

Compensation of a High Speed Photodiode I/V Converter

A classical I/V converter is shown in Figure 4-54. Note that it is the same as the previous photodiode pre-amplifier, if we assume that $R1 \gg R2$. The total input capacitance, C1, is the sum of the diode capacitance and the op amp input capacitance. Dynamically, this is a classical second-order system, and the following guidelines can be applied in order to determine the proper compensation.

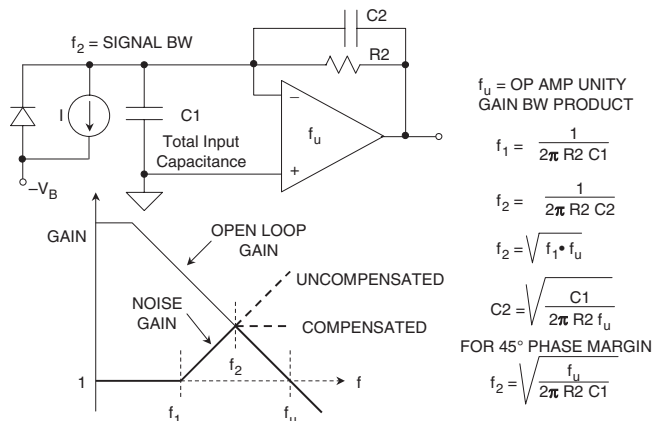


Figure 4-54: Input capacitance compensation for an I/V converter

The net input capacitance, C_1 , forms a zero at a frequency f_1 in the noise gain transfer function as shown in the Bode plot.

$$f_1 = \frac{1}{2\pi R_2 C_1} \quad \text{Eq. 4-6}$$

Note that we are neglecting the effects of the compensation capacitor C_2 and are assuming that it is small relative to C_1 and will not significantly affect the zero frequency f_1 when it is added to the circuit. In most cases, this approximation yields results that are close enough, considering the other variables in the circuit.

If left uncompensated, the phase shift at the frequency of intersection, f_2 , will cause instability and oscillation. Introducing a pole at f_2 by adding the feedback capacitor C_2 stabilizes the circuit and yields a phase margin of about 45 degrees.

$$f_2 = \frac{1}{2\pi R_2 C_2} \quad \text{Eq. 4-7}$$

Since f_2 is the geometric mean of f_1 and the unity-gain bandwidth frequency of the op amp, f_u ,

$$f_2 = \sqrt{f_1 \cdot f_u} \quad \text{Eq. 4-8}$$

These equations can be combined and solved for C_2 :

$$C_2 = \sqrt{\frac{C_1}{2\pi R_2 \cdot f_u}} \quad \text{Eq. 4-9}$$

This C_2 value yields a phase margin of about 45 degrees; increasing it by a factor of 2 increases phase margin to about 65 degrees. In practice, an optimum C_2 value should be determined experimentally, by varying it slightly to optimize the output pulse response.

Op Amp Selection for Wideband Photodiode I/V Converters

The op amp in the high speed photodiode I/V converter should be a wideband FET-input one in order to minimize the effects of input bias current and allow low values of photocurrents to be detected. In addition, if the equation for the 3 dB bandwidth, f_2 , is rearranged in terms of f_u , R_2 , and C_1 , then

$$f_2 = \sqrt{\frac{f_u}{2\pi R_2 C_1}} \quad \text{Eq. 4-10}$$

where C_1 is the sum of the diode capacitance, C_D , and the op amp input capacitance, C_{IN} . In a high speed application, the diode capacitance will be much smaller than that of the low frequency preamplifier design previously discussed—perhaps as low as a few pF.

By inspection of this equation, it is clear that in order to maximize f_2 , the FET-input op amp should have both a high unity gain bandwidth product, f_u , and a low input capacitance, C_{IN} . In fact, the ratio of f_u to C_{IN} is a good figure-of-merit when evaluating different op amps for this application.

Figure 4-55 compares a number of FET-input op amps suitable for photodiode preamps. By inspection, the AD823 op amp has the highest ratio of unity gain bandwidth product to input capacitance, in addition to relatively low input bias current.

For these reasons, the AD823 op amp was chosen for the wideband design.

	Unity GBW Product f_u (MHz)	Input Capacitance C_{IN} (pF)	f_u/C_{IN} (MHz/pF)	Input Bias Current I_B (pA)	Voltage Noise @ 10kHz (nV/ \sqrt{Hz})
AD823	16	1.8	8.9	3	16
AD843	34	6	5.7	600	19
AD744	13	5.5	2.4	100	16
AD845	16	8	2	500	18
OP42	10	6	1.6	100	12
AD745*	20	20	1	250	2.9
AD795	1	1	1	3	8
AD820	1.9	2.8	0.7	10	13
AD743	4.5	20	0.2	250	2.9

*Stable for Noise Gains ≥ 5 , Usually the Case,
Since High Frequency Noise Gain = $1 + C1/C2$,
and $C1$ Usually $\geq 4C2$

Figure 4-55: FET input op amps suitable for high speed photodiode preamps

High Speed Photodiode Preamp Design

The HP 5082-4204 PIN Photodiode will be used as an example for our discussion. Its characteristics are listed in Figure 4-56. It is typical of many PIN photodiodes.

- Sensitivity: 350 μ A @ 1mW, 900nm
- Maximum Linear Output Current: 100 μ A
- Area: 0.002cm² (0.2mm²)
- Capacitance: 4pF @ 10V Reverse Bias
- Shunt Resistance: 10¹¹ Ω
- Risetime: 10ns
- Dark Current: 600pA @ 10V Reverse Bias

Figure 4-56: HP 5082-4204 photodiode characteristics

As in most high speed photodiode applications, the diode will be operated in the reverse-biased or *photo-conductive* mode. This greatly lowers the diode junction capacitance, but causes a small amount of *dark current* to flow even when the diode is not illuminated (we will show a circuit that compensates for the dark current error later in the section). This photodiode is linear with illumination up to approximately 50 μ A to 100 μ A of output current.

The available dynamic range is limited by the total circuit noise, and the diode dark current (assuming no dark current compensation).

Using the circuit shown in Figure 4-57, assume that we wish to have a full scale output of 10 V for a diode current of 100 μA . This determines the value of the feedback resistor R2 to be $10\text{ V}/100\ \mu\text{A} = 100\ \text{k}\Omega$.

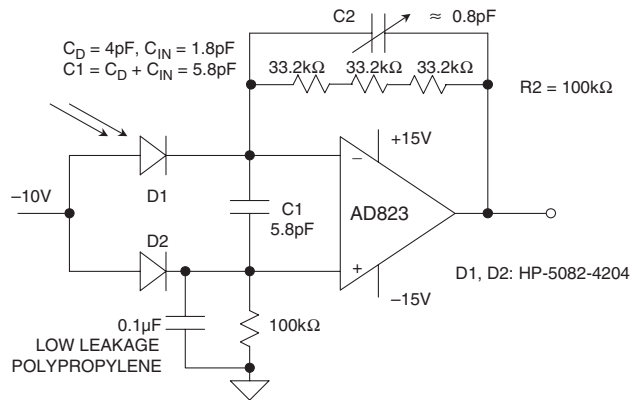


Figure 4-57: 2 MHz bandwidth photodiode preamp with dark current compensation

Using the diode capacitance, $C_D = 4\ \text{pF}$, and the AD823 input capacitance, $C_{IN} = 1.8\ \text{pF}$, the value of $C1 = C_D + C_{IN} = 5.8\ \text{pF}$. Solving the above equations using $C1 = 5.8\ \text{pF}$, $R2 = 100\ \text{k}\Omega$, and $f_u = 16\ \text{MHz}$, we find that:

$$\begin{aligned} f_1 &= 274\ \text{kHz} \\ C2 &= 0.76\ \text{pF} \\ f_2 &= 2.1\ \text{MHz}. \end{aligned}$$

In the final circuit shown, notice at the $100\ \text{k}\Omega$ resistor is replaced with three $33.2\ \text{k}\Omega$ film resistors to minimize stray capacitance. The feedback capacitor, C2, is a variable $1.5\ \text{pF}$ ceramic and is adjusted in the final circuit for best bandwidth/pulse response. The overall circuit bandwidth is approximately 2 MHz.

The full-scale output voltage of the preamp for $100\ \mu\text{A}$ diode current is 10 V, and therefore the (uncompensated) error (RTO) due to the photodiode dark current of $600\ \text{pA}$ is $60\ \mu\text{V}$.

This dark current error can be effectively canceled using a second photodiode, D2, of the same type. This diode is biased with a voltage identical to D1 and, with nominally matched characteristics, will tend to conduct a similar dark current. In the circuit, this “dummy” dark current drives the $100\ \text{k}\Omega$ resistance in the noninverting input of the op amp. This produces a dark current proportional bias voltage which, due to the CM rejection of the op amp, has an end result of suppressing the dark current effects.

High Speed Photodiode Preamp Noise Analysis

As in most noise analyses, only the key contributors need be identified. Because the noise sources combine in an RSS manner, any single noise source that is at least three or four times as large as any of the others will dominate.

In the case of the wideband photodiode preamp, the dominant sources of output noise are the input voltage noise of the op amp, V_N , and the resistor noise due to R2, $V_{N,R2}$ (see Figure 4-58). The input current noise of the FET-input op amp is negligible. The shot noise of the photodiode (caused by the reverse bias) is negligible because of the filtering effect of the shunt capacitance C1.

High Impedance Charge Output Sensors

High impedance transducers such as piezoelectric sensors, hydrophones, and some accelerometers require an amplifier that converts a transfer of charge into a voltage change. Due to the high dc output impedance of these devices, appropriate buffer amplifiers are required. The basic circuit for an inverting charge sensitive amplifier is shown in Figure 4-59.

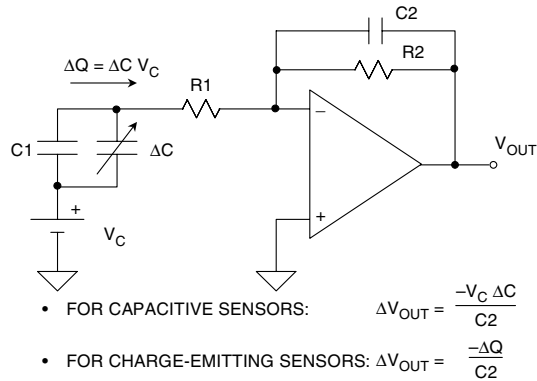


Figure 4-59: Charge amplifier basic principles

There are basically two types of charge transducers: capacitive and charge-emitting. In a capacitive transducer, the voltage across the capacitor (V_c) is held constant. The change in capacitance, ΔC , produces a change in charge, $\Delta Q = \Delta C V_c$. This charge is transferred to the op amp output as a voltage, $\Delta V_{OUT} = -\Delta Q / C2 = -\Delta C V_c / C2$.

Charge-emitting transducers produce an output charge, ΔQ , and their output capacitance remains constant. This charge would normally produce an open-circuit output voltage at the transducer output equal to $\Delta Q / C$. However, since the voltage across the transducer is held constant by the virtual ground of the op amp ($R1$ is usually small), the charge is transferred to capacitor C_2 producing an output voltage $\Delta V_{OUT} = -\Delta Q / C2$. In an actual application, this charge amplifier only responds to ac inputs.

It should be noted that ac gain for this charge amplifier is determined by the *capacitance ratio*, not the resistances. This is unlike a conventional wideband amplifier, where the upper cutoff frequency is given by $f_2 = 1/2 \pi R2 C2$, and the lower by $f_1 = 1/2 \pi R1 C1$.

In the Figure 4-59 charge amplifier, with nominal transducer capacitance fixed, gain is set by $C2$. Typically, bias return resistor $R2$ will be a high value (≥ 1 meg Ω), and $R1$ a much lower value. The resulting frequency response will be relatively narrow and bandpass shaped, with gain and frequency manipulated by the relative values, as suitable to SPICE analysis.

Low Noise Charge Amplifier Circuit Configurations

Figure 4-60 shows two ways to buffer and amplify the output of a charge output transducer. Both require using an amplifier which has a very high input impedance, such as the AD745. The AD745 provides both low voltage noise and low current noise. This combination makes this device particularly suitable in applications requiring very high charge sensitivity, such as capacitive accelerometers and hydrophones.

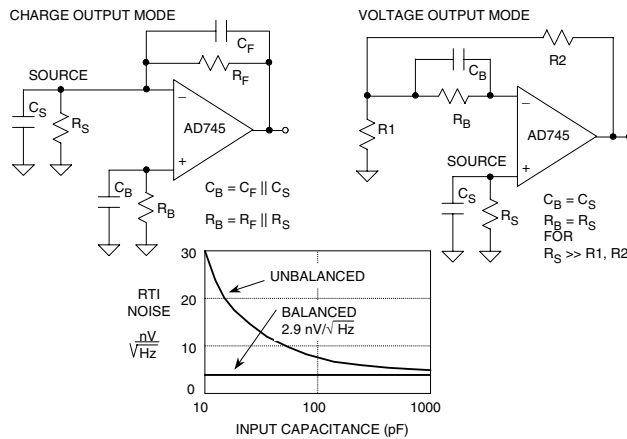


Figure 4-60: Two basic charge amplifier configurations using the AD745 low noise FET op amp

The first (left) circuit in Figure 4-60 uses the op amp in the inverting mode. Amplification depends on the principle of conservation of charge at the inverting input of the amplifier. The charge on capacitor C_S is transferred to capacitor C_F , thus yielding an output voltage of $\Delta Q/C_F$. The amplifier's input voltage noise will appear at the output amplified by the ac noise gain of the circuit, $1 + C_S/C_F$.

The second (right) circuit shown in Figure 4-60 is simply a high impedance follower with gain. Here the noise gain ($1 + R_2/R_1$) is the same as the gain from the transducer to the output. Resistor R_B , in both circuits, is required as a dc bias current return.

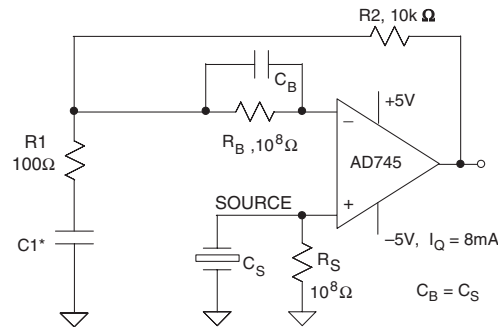
To maximize dc performance over temperature, source resistances should be balanced at the amplifier inputs, as represented by the resistor R_B shown in Figure 4-60. For best noise performance, the source capacitance should also be balanced with the capacitor C_B .

In general, it is good practice to balance the source impedances (both resistive and reactive) as seen by the inputs of precision low noise BiFET amplifiers such as the AD743/AD745. Balancing the resistive components will optimize dc performance over temperature, as balancing mitigates the effects of any bias current errors. Balancing the input capacitance will minimize ac response errors due to the amplifier's nonlinear common-mode input capacitance and, as shown in Figure 4-60, noise performance will be optimized. In any FET input amplifier, the current noise of the internal bias circuitry can be coupled to the inputs via the gate-to-source capacitances (20 pF for the AD743 and AD745) and appears as excess input voltage noise. This noise component is correlated at the inputs, so source impedance matching will tend to cancel out its effect. Figure 4-60 shows the required external components for both inverting and noninverting configurations. For values of C_B greater than 300 pF, there is a diminishing impact on noise, and C_B can then be simply a polyester bypass capacitor of 0.01 μF or greater.

40dB Gain Piezoelectric Transducer Amplifier Operates on Reduced Supply Voltages for Lower Bias Current

Figure 4-61 shows a gain-of-100 piezoelectric transducer amplifier connected in the voltage-output mode. Reducing the op amp power supplies to $\pm 5\text{ V}$ reduces the effects of bias current in two ways: first, by lowering the total power dissipation and, second, by reducing the basic gate-to-junction leakage current. The addition of a clip-on heat sink such as the Aavid #5801 will further limit the internal junction temperature rise.

With ac coupling capacitor C1 shorted, the amplifier will operate over a range of 0°C to 85°C . If the optional ac coupling capacitor C1 is used, the circuit will operate over the entire -55°C to $+125^\circ\text{C}$ temperature range, but dc information is lost.



- $\pm 5\text{V}$ Power Supplies Reduce I_B for 0°C to $+85^\circ\text{C}$ Operation, $P_D = 80\text{mW}$
- C1 Allows -55°C to $+125^\circ\text{C}$ Operation

Figure 4-61: A gain-of-100 piezoelectric transducer amplifier

Hydrophones

Interfacing the outputs of highly capacitive transducers such as hydrophones, some accelerometers, and condenser microphones to the outside world presents many design challenges. Previously designers had to use costly hybrid amplifiers consisting of discrete low-noise JFETs in front of conventional op amps to achieve the low levels of voltage and current noise required by these applications. Using AD743/AD745 monolithic ICs, designers can achieve almost the same level of performance of a hybrid approach.

In sonar applications, a piezo-ceramic cylinder is commonly used as the active element in the hydrophone. A typical cylinder has a nominal capacitance of around 6,000 pF with a series resistance of $10\ \Omega$. The output impedance is typically $10^8\ \Omega$ or $100\ \text{M}\Omega$.

Since the hydrophone signals of interest are inherently ac with wide dynamic range, noise is an overriding concern for sonar system designs. The noise floor of the hydrophone and its preamplifier together limit the system sensitivity, and thus the overall hydrophone usefulness. Typical hydrophone bandwidths are in the 1 kHz to 10 kHz range. The AD743 and AD745 op amps, with their low noise voltages of $2.9\text{nV}/\sqrt{\text{Hz}}$ and high input impedance of $10^{10}\ \Omega$ (or $10\ \text{G}\Omega$) are ideal for use as hydrophone amplifiers.

Op Amp Performance: JFET versus Bipolar

The AD743 and AD745 op amps are the first monolithic JFET devices to offer the low input voltage noise comparable to a bipolar op amp, *without* the high input bias currents typically associated with bipolar op amps. Figure 4-62 shows input voltage noise versus input source resistance of the OP27 (bipolar-input) and the JFET-input AD745 op amps. Note: the noise levels of the AD743 and the AD745 are identical.

From this figure (left), it is clear that at high source impedances, the low current noise of the AD745 provides lower overall noise than a high performance bipolar op amp such as the OP27. It is also important to note that, with the AD745, this noise reduction extends down to low source impedances. At high source impedances, the lower dc current errors of the AD745 also reduce errors due to offset and drift, as shown in Figure 4-62 (right).

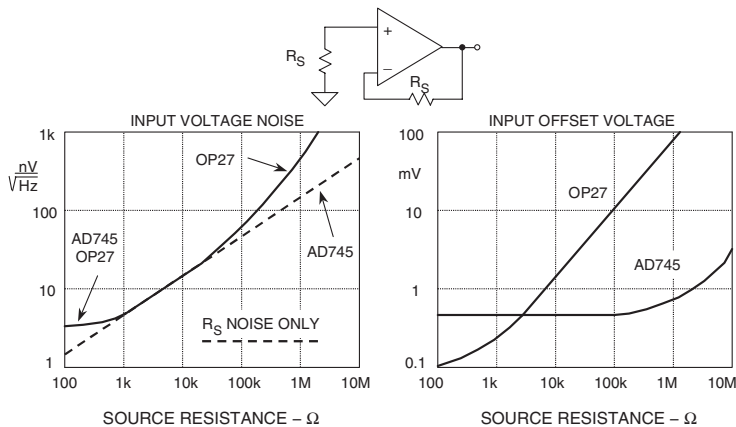


Figure 4-62: Total noise performance comparison, OP27 (bipolar) and AD745 (FET) op amps

The AD743 and AD745 are related, companion amplifiers, which differ in their levels of internal compensation. The AD743 is internally compensated for unity gain stability. The AD745, stable for noise gains of 5 or higher, has a much higher bandwidth and slew rate. This makes the latter device especially useful as a high-gain preamplifier where it provides both high gain and wide bandwidth. The AD743 and AD745 also operate with very low levels of distortion; less than 0.0003% and 0.0002% (at 1 kHz), respectively.

A pH Probe Buffer Amplifier

A typical pH probe requires a buffer amplifier to isolate its 10^6 to $10^9 \Omega$ source resistance from external circuitry. Such an amplifier is shown in Figure 4-63. The low input current of the AD795JR minimizes the voltage error produced by the bias current and electrode resistance. The use of guarding, shielding, high insulation resistance standoffs, and other such standard picoamp methods previously discussed should be used to minimize leakage. Are all needed to maintain the accuracy of this circuit.

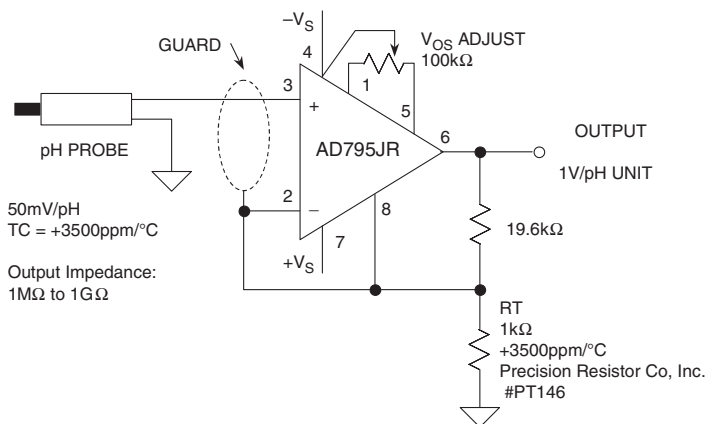


Figure 4-63: A gain of 20x pH probe amplifier allows 1 V/pH output scaling

The slope of the pH probe transfer function, 50 mV per pH unit at room temperature, has an approximate +3500 ppm/°C temperature coefficient. The buffer amplifier shown as Figure 4-63 provides a gain of 20, and yields a final output voltage equal to 1 V/pH unit. Temperature compensation is provided by resistor RT, which is a special temperature compensation resistor, 1 kΩ, 1%, +3500 ppm/°C, #PT146 available from Precision Resistor Co., Inc. (see Reference 15).

References: High Impedance Sensors

1. Ramon Pallas-Areny and John G. Webster, **Sensors and Signal Conditioning**, John Wiley, New York, 1991.
2. Dan Sheingold, Editor, **Transducer Interfacing Handbook**, Analog Devices, Inc., 1980, ISBN: 0-916550-05-2.
3. Section 3, Walt Kester, Editor, **1992 Amplifier Applications Guide**, Analog Devices, 1992, ISBN: 0-916550-10-9.
4. Walt Kester, Editor, **System Applications Guide**, Analog Devices, 1993, ISBN: 0-916550-13-3.
5. Walt Kester, Editor, **Linear Design Seminar**, Analog Devices, 1995, ISBN: 0-916550-15-X.
6. Walt Kester, Editor, **Practical Analog Design Techniques**, Analog Devices, 1995, ISBN: 0-916550-16-8.
7. Walt Kester, Editor, **High Speed Design Techniques**, Analog Devices, 1996, ISBN: 0-916550-17-6.
8. Jiri Dostal, Section 9.3.1, "Thermoelectric Voltages," **Operational Amplifiers 2nd Ed.**, Butterworth-Heinemann, 1993, pp. 265–268.
9. Optoelectronics Data Book, EG&G Vactec, St. Louis, MO, 1990.
10. Silicon Detector Corporation, Camarillo, CA, Part Number SD-020-12-001 Data Sheet.
11. Photodiode 1991 Catalog, Hamamatsu Photonics, Bridgewater, NJ.
12. Lewis Smith and Dan Sheingold, "Noise and Operational Amplifier Circuits," **Analog Dialogue 25th Anniversary Issue**, pp. 19–31, Analog Devices Inc., 1991.
13. James L. Melsa and Donald G. Schultz, **Linear Control Systems**, pp. 196–220, McGraw-Hill, 1969.
14. Jerald G. Graeme, **Photodiode Amplifiers: Op Amp Solutions**, McGraw-Hill, 1995.
15. Precision Resistor Co., Inc., 10601 75th St. N., Largo, FL, 33777-1427, 727 541-5771, www.precisionresistor.com.
16. **Ohmite Victoreen MAXI-MOX Resistors**, 3601 Howard Street, Skokie, IL 60076, 847 675-2600, www.ohmite.com/victoreen/.
17. **Vishay/Dale RNX Resistors**, 2300 Riverside Blvd., Norfolk, NE, 68701-2242, 402 371-0800, www.vishay.com.

This page intentionally left blank

Temperature Sensors

Walt Kester, James Bryant, Walt Jung

Temperature measurement is critical in many modern electronic devices, especially expensive laptop computers and other portable devices; their densely packed circuitry dissipates considerable power in the form of heat. Knowledge of system temperature can also be used to control battery charging, as well as to prevent damage to expensive microprocessors.

Compact high power portable equipment often has fan cooling to maintain junction temperatures at proper levels. In order to conserve battery life, the fan should only operate when necessary. Accurate control of the fan requires, in turn, knowledge of critical temperatures from an appropriate temperature sensor.

Accurate temperature measurements are required in many other measurement systems, for example within process control and instrumentation applications. Some popular types of temperature transducers and their characteristics are indicated in Figure 4-64. In most cases, because of low level and/or nonlinear outputs, the sensor output must be properly conditioned and amplified before further processing can occur.

THERMOCOUPLE	RTD	THERMISTOR	SEMICONDUCTOR
Widest Range: -184°C to +2300°C	Range: -200°C to +850°C	Range: 0°C to +100°C	Range: -55°C to +150°C
High Accuracy and Repeatability	Fair Linearity	Poor Linearity	Linearity: 1°C Accuracy: 1°C
Needs Cold Junction Compensation	Requires Excitation	Requires Excitation	Requires Excitation
Low-Voltage Output	Low Cost	High Sensitivity	10mV/K, 20mV/K, or 1µA/K Typical Output

Figure 4-64: Some common types of temperature transducers

Except for the semiconductor sensors of the last column, all of the temperature sensors shown have non-linear transfer functions. In the past, complex analog conditioning circuits were designed to correct for the sensor nonlinearity. These circuits often required manual calibration and precision resistors to achieve the desired accuracy. Today, however, sensor outputs may be digitized directly by high resolution ADCs. Linearization and calibration can then be performed digitally, substantially reducing cost and complexity.

Resistance Temperature Devices (RTDs) are accurate, but require excitation current and are generally used within bridge circuits such as those described earlier. *Thermistors* have the most sensitivity, but are also the most nonlinear. Nevertheless, they are popular in portable applications for measurement of battery and other critical system temperatures.

Modern *semiconductor temperature sensors* offer both high accuracy and linearity over about a -55°C to $+150^{\circ}\text{C}$ operating range. Internal amplifiers can scale output to convenient values, such as $10\text{ mV}/^{\circ}\text{C}$. They are also useful in cold-junction compensation circuits for wide temperature range thermocouples. Semiconductor temperature sensors are also integrated into ICs that perform other hardware monitoring functions—an example is the imbedded transistor sensors used within modern μP chips.

Thermocouple Principles and Cold-Junction Compensation

Thermocouples comprise a more common form of temperature measurement. In operation, thermocouples rely on the fact that two dissimilar metals joined together produce a voltage output roughly proportional to temperature. They are small, rugged, relatively inexpensive, and operate over the widest range of contact temperature sensors.

Thermocouples are especially useful for making measurements at extremely high temperatures (up to $+2300^{\circ}\text{C}$), and within hostile environments. Characteristics of some common types are shown in Figure 4-65.

JUNCTION MATERIALS	TYPICAL USEFUL RANGE ($^{\circ}\text{C}$)	NOMINAL SENSITIVITY ($\mu\text{V}/^{\circ}\text{C}$)	ANSI DESIGNATION
Platinum (6%)/Rhodium-Platinum (30%)/Rhodium	38 to 1800	7.7	B
Tungsten (5%)/Rhenium-Tungsten (26%)/Rhenium	0 to 2300	16	C
Chromel-Constantan	0 to 982	76	E
Iron-Constantan	0 to 760	55	E
Chromel-Alumel	-184 to 1260	39	K
Platinum (13%)/Rhodium-Platinum	0 to 1593	11.7	R
Platinum (10%)/Rhodium-Platinum	0 to 1538	10.4	S
Copper-Constantan	-184 to 400	45	T

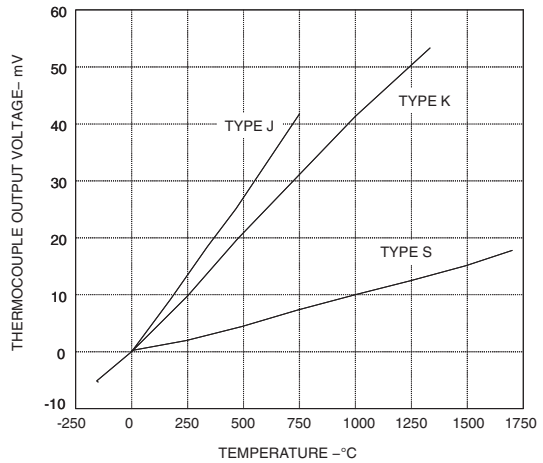
Figure 4-65: Some common thermocouples and their characteristics

However, thermocouples produce only millivolts of output, and thus they typically require precision amplification for further processing. They also require *cold-junction-compensation* (CJC) techniques, to be discussed shortly. They are more linear than many other sensors, and their nonlinearity has been well characterized.

The most common metals used for thermocouples are iron, platinum, rhodium, rhenium, tungsten, copper, alumel (composed of nickel and aluminum), chromel (composed of nickel and chromium) and constantan (composed of copper and nickel).

Figure 4-66 shows the voltage-temperature curves for three commonly used thermocouples, Types J, K, and S, referred to a 0°C fixed-temperature reference junction. Of these, Type J thermocouples are the most sensitive, producing the highest output voltage for a given temperature change, but over a relatively narrow temperature span. On the other hand, Type S thermocouples are the least sensitive, but can operate over a much wider range.

Figure 4-66: Type J, K, and S thermocouple output voltage versus temperature



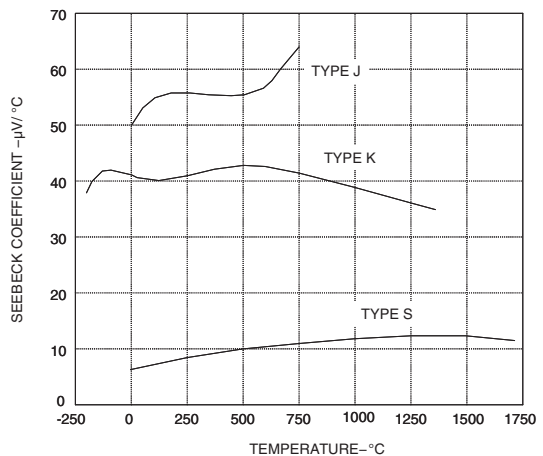
These characteristics are very important considerations when designing thermocouple signal conditioning circuitry. A main consideration is the fact that virtually any thermocouple employed will have a relatively low output signal, thus they generally require the careful application of stable, high gain amplifiers.

To understand thermocouple behavior more fully, it is also necessary to consider the nonlinearities in their response to temperature differences. As noted, Figure 4-66 shows the relationships between sensing junction temperature and voltage output for a number of thermocouple types (in all cases, the reference *cold* junction is maintained at 0°C).

While close scrutiny of these data may reveal the fact that none of the responses are quite linear, the exact nature of the nonlinearity isn't so obvious. What is needed is another perspective on the relationships displayed by these curves, to gain better insight into how the various devices can be best utilized.

Figure 4-67 shows how the thermocouple *Seebeck* coefficient varies with sensor junction temperature. The Seebeck coefficient is the *change* of output voltage with *change* of sensor junction temperature (i.e., the first derivative of output with respect to temperature). Note that we are still considering the case where the reference junction is maintained at 0°C.

Figure 4-67: Type J, K and S thermocouple Seebeck coefficient versus temperature



An ideal linear thermocouple would have a constant Seebeck coefficient with varying temperature, but in practice all thermocouples are nonlinear to some degree. In selecting a measurement thermocouple for a particular temperature range, we should therefore choose one whose Seebeck coefficient varies as little as possible over that range.

For example, a Type J thermocouple has a nominal Seebeck coefficient of $55 \mu\text{V}/^\circ\text{C}$, which varies by less than $1 \mu\text{V}/^\circ\text{C}$ between 200°C and 500°C , making it ideal for measurements over this range (the flat region of the upper curve within Figure 4-67).

Presenting these data on thermocouples serves two purposes. First, Figure 4-66 illustrates the range and sensitivity of the three thermocouple types so that the system designer can, at a glance, determine that a Type S thermocouple has the widest useful temperature range, but a Type J thermocouple is the more sensitive of the three.

Second, the relative stability of the Seebeck coefficient over temperature provides a quick guide to a thermocouple's linearity. Using Figure 4-67, a system designer can choose a Type K thermocouple for its relatively linear Seebeck coefficient over the range of 400°C to 800°C , or a Type S over the range of 900°C to 1700°C . The behavior of a thermocouple's Seebeck coefficient is important in applications where variations of temperature rather than absolute magnitude are important. These data also indicate what performance is required of the associated signal-conditioning circuitry.

To successfully apply thermocouples we must also understand their basic operating principles. Consider the diagrams shown in Figure 4-68.

If we join two dissimilar metals, A and B, at any temperature above absolute zero, there will be a potential difference between them, i.e., their "thermoelectric EMF" or "contact potential," V_1 . This voltage is a function of the temperature of the measurement junction, T_1 , as is noted in Figure 4-68A. If we join two wires of metal A with metal B at two places, two measurement junctions are formed, T_1 and T_2 (Figure 4-68B). If the two junctions are at different temperatures, there will be a net EMF in the circuit, and a current I will flow, as determined by the EMF $V_1 - V_2$, and the total resistance R in the circuit (Figure 4-68B).

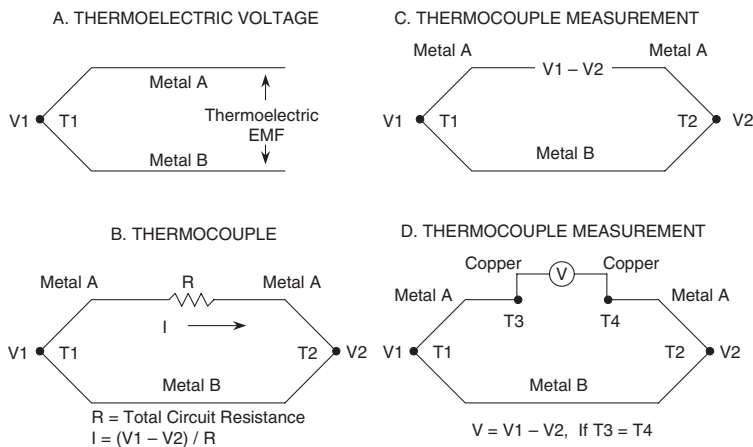


Figure 4-68: Thermocouple basics

If we open the circuit as in Figure 4-68C, the voltage across the break will be equal to the net thermoelectric EMF of the circuit; and if we measure this voltage, we can use it to calculate the temperature difference between the two junctions. We must remember that a thermocouple always measures the temperature *difference* between two junctions, not the absolute temperature at one junction. We can only measure the temperature at the measuring junction if we know the temperature of the other junction. This is the origin of the terms “reference” or “cold” junction.

But of course, it is not so easy to just measure the voltage generated by a thermocouple. *Any wire attached to a thermocouple is also a thermocouple itself*, and if care is not taken, errors can be introduced. Suppose that we attach a voltmeter to the circuit of Figure 4-68C, as shown in Figure 4-68D. The wires of the voltmeter will form further thermocouple junctions where they are attached (T_3 , T_4). If both these additional junctions are at the same temperature (it does not matter exactly what temperature), then the “Law of Intermediate Metals” states that they will make no net contribution to the total EMF of the system. If they are at different temperatures, they will introduce errors.

Since *every pair of dissimilar metals in contact generates a thermoelectric EMF* (including copper/solder, kovar/copper [kovar is the alloy used for IC leadframes] and aluminum/kovar [at the bond inside the IC]), it is obvious that in practical circuits the problem is even more complex. In fact, it is necessary to take extreme care to ensure that both junctions of each junction pair in series with a thermocouple are at the same temperature, *except for the measurement and reference junctions themselves*.

Thermocouples generate a voltage, albeit a very small one, and don’t require excitation for this most basic operation. As was shown in Figure 4-68D, however, two junctions are always involved (T_1 , the measurement junction temperature and T_2 , the reference junction temperature). If $T_2 = T_1$, then $V_2 = V_1$, and the output voltage $V = 0$. Thermocouple output voltages are often defined with respect to a reference junction temperature of 0°C (hence the term *cold* or *ice point* junction). In such a system the thermocouple provides a convenient output voltage of 0 V at 0°C . Obviously, to maintain system accuracy, the reference junction must remain at a well-defined temperature (but not necessarily 0°C).

A conceptually simple approach to this need is shown in Figure 4-69, the ice-point reference, where junction T_2 is kept at 0°C by virtue of being immersed in an ice water slurry. Although this ice water bath is relatively easy to define conceptually, it is quite inconvenient to maintain.

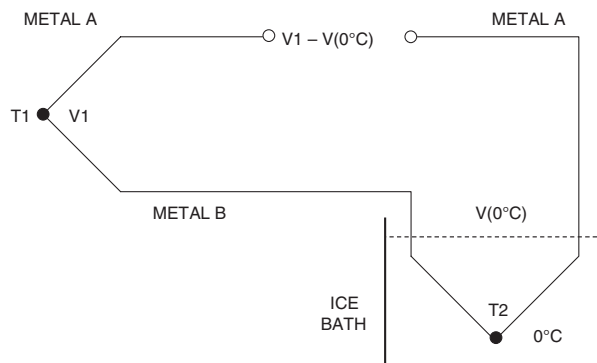


Figure 4-69: A thermocouple cold junction reference system using an ice-point (0°C) T_2 reference

Today the inconvenient ice/water bath reference is replaced by an electronic equivalent. A temperature sensor of another sort (often a semiconductor sensor, sometimes a thermistor) measures the cold junction temperature and is used to inject a voltage into the thermocouple circuit which compensates for the difference between the actual cold junction temperature and its ideal value (usually 0°C) as shown in Figure 4-70.

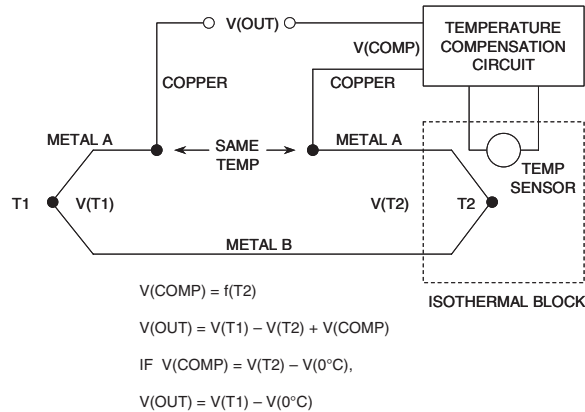
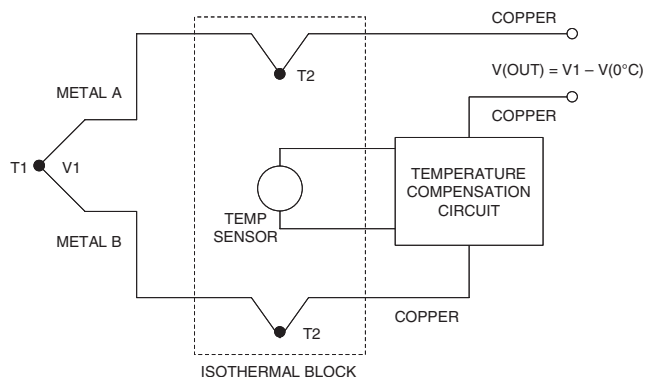


Figure 4-70: A semiconductor temperature sensor can be used to provide cold junction compensation

Ideally, the compensation voltage should be an exact match for the difference voltage required, which is why the diagram gives the voltage $V(\text{COMP})$ as $f(T_2)$ (a function of T_2) rather than KT_2 , where K is a simple constant. In practice, since the cold junction is rarely more than a few tens of degrees from 0°C, and generally varies by little more than $\pm 10^\circ\text{C}$, a linear approximation ($V = KT_2$) to the more complex reality is usually sufficiently accurate and is often used. (Note—the expression for the output voltage of a thermocouple with its measuring junction at $T^\circ\text{C}$ and its reference at 0°C is a polynomial of the form $V = K_1T + K_2T^2 + K_3T^3 + \dots$, but the values of the coefficients K_2 , K_3 , and so forth, are very small for most common types of thermocouple). References 7 and 8 give the values of these coefficients for a wide range of thermocouples.

When electronic cold-junction compensation is used, it is common practice to eliminate the additional thermocouple wire, and terminate the thermocouple leads in the isothermal block, as shown in the arrangement of Figure 4-71.

Figure 4-71: Termination of thermocouple leads directly to an isothermal block



In Figure 4-71, the Metal A-Copper and the Metal B-Copper junctions, if at temperature T_2 , are equivalent to the Metal A-Metal B thermocouple junction in Figure 4-70.

Type K Thermocouple Amplifier and Cold Junction Compensator

The circuit in Figure 4-72 conditions the output of a Type K thermocouple, while providing cold-junction compensation, operating over temperatures between 0°C and 250°C . The circuit operates from single $+3.3\text{ V}$ to $+5.5\text{ V}$ supplies with the AD8551, and has been designed to produce a basic output voltage transfer characteristic of $10\text{ mV}/^\circ\text{C}$. A Type K thermocouple exhibits a Seebeck coefficient of approximately $40\text{ }\mu\text{V}/^\circ\text{C}$; therefore, at the cold junction, the TMP35 voltage output sensor with a temperature coefficient of $10\text{ mV}/^\circ\text{C}$ is used with divider R1 and R2, to introduce an opposing cold-junction temperature coefficient of $-40\text{ }\mu\text{V}/^\circ\text{C}$. This prevents the isothermal, cold-junction connection between the circuit's printed circuit board traces and the thermocouple's wires from introducing an error in the measured temperature. This compensation works extremely well for conditioning circuit ambient temperatures of 20°C to 50°C .

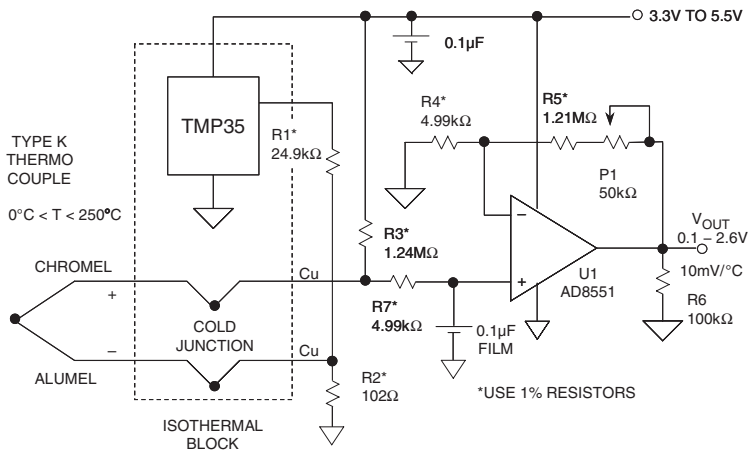


Figure 4-72: Using a TMP35 temperature sensor for cold junction compensation within a Type K thermocouple amplifier-conditioner

Over a 250°C measurement temperature range, the thermocouple produces an output voltage change of $\sim 10\text{ mV}$. Since the circuit's required full-scale output voltage change is 2.5 V , the required gain is ~ 250 . Choosing R4 equal to $4.99\text{ k}\Omega$ sets R5 $\sim 1.24\text{ M}\Omega$. With a fixed 1% value for R5 of $1.21\text{ M}\Omega$, a $50\text{ k}\Omega$ potentiometer is used with R5 for fine trim of the full-scale output voltage. The U1 amplifier should be a low drift, very high gain type. A chopper-stabilized AD8551 or an OP777 precision bipolar op amp is suitable for U1.

Both the AD8551 and the OP777 have rail-rail output stages. To extend low range linearity, bias resistor R3 is added to the circuit, supplying an output offset voltage of about 0.1 V (for a nominal supply voltage of 5 V). Note that this 10°C offset must be subtracted, when making final measurements referenced to the U1 output. Note also that R3 provides a useful open thermocouple detection function, forcing the U1 output to greater than 3 V should the thermocouple open. Resistor R7 balances the dc input impedance at the U1 (+) input, and the $0.1\text{ }\mu\text{F}$ film capacitor reduces noise coupling.

Single-Chip Thermocouple Signal Conditioners

While the construction of thermocouple signal conditioners with op amps and other discrete circuit elements offers great flexibility, this does come at the expense of component count. To achieve a greater level of integration in the thermocouple conditioning function, dedicated thermocouple signal conditioners can be used.

One such solution lies with the AD594 and AD595 (see Reference 9), which are complete, single-chip instrumentation amplifiers and thermocouple cold junction compensators, as shown in Figure 4-73. Suitable for use with either Type J (AD594) or Type K (AD595) thermocouples, these two devices combine an ice point reference with a precalibrated scaling amplifier. They provide a high level ($10 \text{ mV}/^\circ\text{C}$) output working directly from a thermocouple input, without additional precision parts. Pin-strapping options allow the devices to be used as a linear amplifier-compensator, or as a switched output set-point controller with fixed or remote setpoint control.

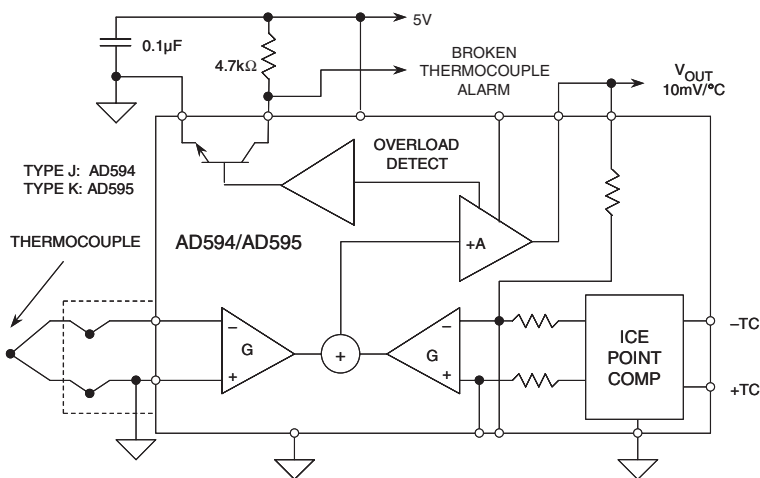


Figure 4-73: Functional diagram of AD594 and AD595 thermocouple signal-conditioning amplifiers

The AD594 and AD595 can be used to amplify the cold-junction compensation voltage directly, thereby becoming a standalone, $10 \text{ mV}/^\circ\text{C}$ output Celsius transducer. In such applications it is very important that the IC chip be at the same temperature as the cold junction of the thermocouple; this is usually achieved by keeping the two in close proximity and isolated from any heat sources.

The AD594/AD595 structure includes a flexible thermocouple failure alarm output, which provides broken thermocouple indication. The devices can be powered from either dual or single power supplies (as low as 5 V), but the use of a negative supply also allows temperatures below 0°C to be measured. To minimize self-heating, an unloaded AD594/AD595 operates with $160 \mu\text{A}$ of supply current, and can deliver $\pm 5 \text{ mA}$ to a load.

Although the AD594 is precalibrated by laser wafer trimming to match the characteristics of Type J thermocouples, and the AD595 for Type K, the temperature transducer voltages and gain control resistors are also made available at the package pins. So, if desired, the circuit can be recalibrated for other thermocouple types with the addition of external resistors. These terminals also allow more precise calibration for both

thermocouple and thermometer applications. The AD594/AD595 are available in C and A performance grades, with calibration accuracies of $\pm 1^\circ\text{C}$ and $\pm 3^\circ\text{C}$, respectively. Both are designed to be used with cold junctions between 0 to 50°C .

The 5 V powered, single-supply circuit shown of Figure 4-73 provides a scaled $10\text{ mV}/^\circ\text{C}$ output capable of measuring a range of 0°C to 300°C . This can be from either a Type J thermocouple using the AD594, or a Type K with the AD595.

Resistance Temperature Detectors

The Resistance Temperature Detector (RTD), is a sensor whose resistance changes with temperature. Typically built of a platinum (Pt) wire wrapped around a ceramic bobbin, the RTD exhibits behavior which is more accurate and more linear than a thermocouple over wide temperature ranges.

Figure 4-74 illustrates the temperature coefficient of a $100\ \Omega$ RTD, and the Seebeck coefficient of a Type S thermocouple. Over the entire range (approximately -200°C to $+850^\circ\text{C}$), the RTD is a more linear device. Hence, linearizing an RTD is less complex.

- Platinum (Pt) the Most Common
- $100\ \Omega$, $1000\ \Omega$ Standard Values
- Typical TC = $0.385\%/^\circ\text{C}$
= $0.385\ \Omega/^\circ\text{C}$ for $100\ \Omega$ Pt RTD
- Good Linearity – Better than Thermocouple,
- Easily Compensated

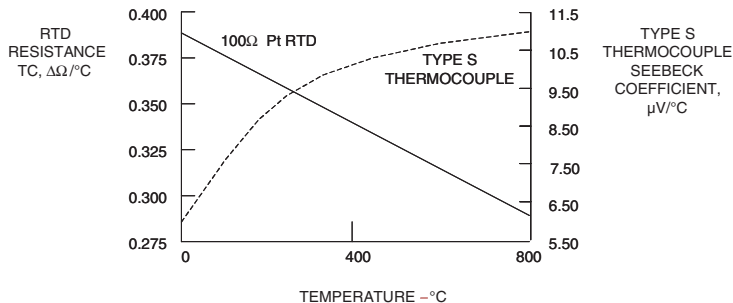


Figure 4-74: Resistance temperature detectors

Unlike a thermocouple, however, an RTD is a passive sensor, and a current excitation is required to produce an output voltage. The RTD's low temperature coefficient of $0.385\%/^\circ\text{C}$ requires high performance signal-conditioning circuitry similar to that used by a thermocouple. However, the typical voltage drop seen across an RTD is much larger than a thermocouple's output voltage. A system designer may opt for large value RTDs with higher output, but large-valued RTDs exhibit slow response times. Furthermore, although the cost of RTDs is higher than that of thermocouples, they use copper leads, and thermoelectric effects from terminating junctions do not affect their accuracy. And finally, because their resistance is a function of the absolute temperature, RTDs do not require cold-junction compensation.

Caution must be exercised with the level of current excitation applied to an RTD, because excessive current can cause self-heating. Any self-heating changes the RTD temperature, and therefore results in a measurement error. Hence, careful attention must be paid to the design of the signal-conditioning circuitry so that

self-heating errors are kept below 0.5°C . Manufacturers specify self-heating errors for various RTD values and sizes, in both still and moving air. To reduce the error due to self-heating, the minimum current should be used to achieve the required system resolution, and the largest RTD value chosen that results in acceptable response time.

Another effect that can produce measurement error is voltage drop in RTD lead wires. This is especially critical with low value, 2-wire RTDs, because both the temperature coefficient and absolute value of the RTD resistance are small. If the RTD is located a long distance from the signal-conditioning circuitry, the connecting lead resistance can be ohms or tens of ohms. Even this small amount of lead resistance can contribute a significant error to the temperature measurement, as shown in Figure 4-75.

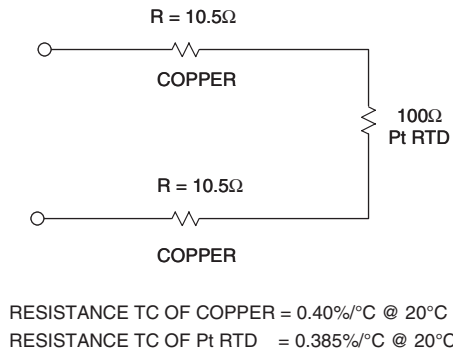


Figure 4-75: A $100\ \Omega$ Pt RTD with 100-foot #30 AWG lead wires

To illustrate this point, assume that a $100\ \Omega$ platinum RTD with 30-gage copper leads is located about 100 feet from a controller’s display console. The resistance of 30-gage copper wire is $0.105\ \Omega/\text{ft}$, and the two leads of the RTD will contribute a total $21\ \Omega$ to the network. Uncorrected, this additional resistance will produce a 55°C measurement error. Obviously, the temperature coefficient of the connecting leads can contribute an additional, and possibly significant, error to the measurement.

To eliminate the effect of the lead resistance, a 4-wire technique is used. In Figure 4-76, a 4-wire (Kelvin) connection is made to the RTD. A constant current, I , is applied through the FORCE leads of the RTD, and the voltage across the RTD itself is measured remotely, via the SENSE leads. The measuring device can be a DVM or an in amp, and high accuracy can be achieved provided that the measuring device exhibits high

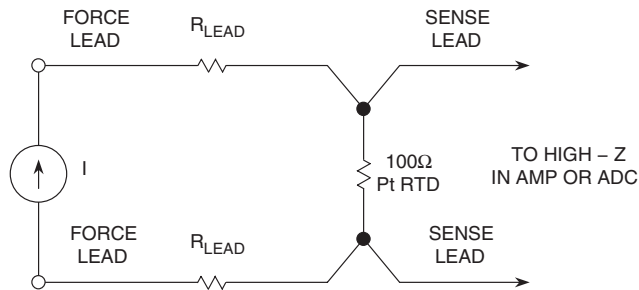


Figure 4-76: Use of Kelvin or 4-wire Pt RTD connections provides high accuracy

input impedance and/or low input bias current. Since the SENSE leads don't carry appreciable current, this technique is relatively insensitive to lead wire length. Some major sources of errors in this scheme are the stability of the constant current source, and the input impedance and/or bias currents in the amplifier or DVM, and the associated drift.

RTDs are generally configured in a four-resistor bridge circuit. The bridge output is amplified by an in amp for further processing. However, high resolution measurement ADCs allow the RTD output to be digitized directly. In this manner, linearization can be performed digitally, thereby easing the analog circuit requirements considerably.

For example, an RTD output can be digitized by one of the AD77xx series high resolution ADCs. Figure 4-77 shows a $100\ \Omega$ Pt RTD, driven with a $400\ \mu\text{A}$ excitation current source. Note that the $400\ \mu\text{A}$ RTD excitation current source also generates a $2.5\ \text{V}$ reference voltage for the ADC, by virtue of flowing in a $6.25\ \text{k}\Omega$ resistor, R_{REF} , with the drop across this resistance being metered by the ADC's V_{REF} (+) and (-) input terminals.

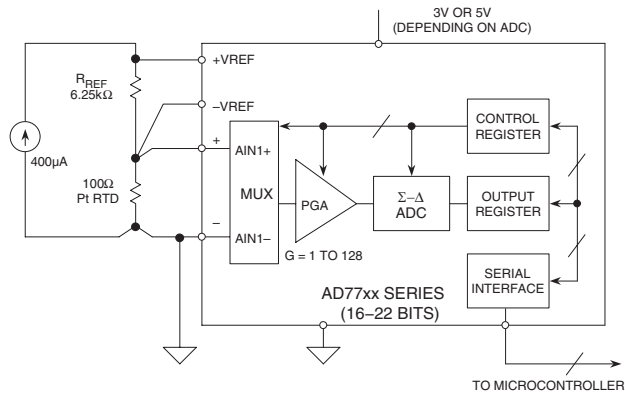


Figure 4-77: A Pt RTD interfaced to the AD77xx series of high resolution ADCs

It should be noted that this simple scheme has great benefits (beyond the obvious one of simplicity). Variations in the magnitude of the $400\ \mu\text{A}$ excitation current do not affect circuit accuracy, since both the input voltage drop across the RTD as well as the reference voltage across R_{REF} vary ratiometrically with the excitation current. However, it should be noted that the $6.25\ \text{k}\Omega$ resistor must be a stable type with a low temperature coefficient, to avoid errors in the measurement. Either a wirewound resistor, or a very low TC metal film type is most suitable for R_{REF} within this application.

In this application, the ADC's high resolution and the gain of 1 to 128 input PGA eliminates the need for any additional conditioning. The high resolution ADC can in fact perform virtually all the conditioning necessary for an RTD, leaving any further processing such as linearization to be performed in the digital domain.

Thermistors

Similar in general function to RTDs, thermistors are low-cost temperature-sensitive resistors, constructed of solid semiconductor materials which exhibit a positive or negative temperature coefficient. Although positive temperature coefficient devices do exist, the most common thermistors are negative temperature coefficient (NTC) devices.

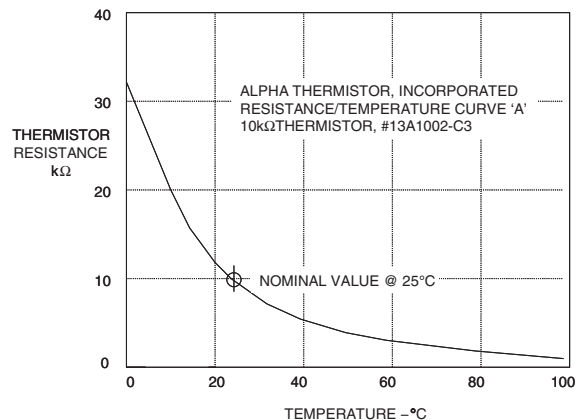


Figure 4-78: Resistance characteristics for a 10kΩ NTC thermistor

Figure 4-78 shows the resistance-temperature characteristic of a commonly used NTC thermistor. Although the thermistor is the most nonlinear of the three temperature sensors discussed, it is also the most sensitive.

The thermistor's very high sensitivity (typically $-44,000$ ppm/°C at 25°C) allows it to detect minute temperature variations not readily observable with an RTD or thermocouple. This high sensitivity is a distinct advantage over the RTD, in that 4-wire Kelvin connections to the thermistor aren't needed for lead wire error compensation. To illustrate this point, suppose a 10 kΩ NTC thermistor with a typical 25°C temperature coefficient of $-44,000$ ppm/°C were substituted for the 100 Ω Pt RTD in the example given earlier. The total lead wire resistance of 21 Ω would generate less than 0.05°C error in the measurement, using the thermistor in lieu of the RTD. This is roughly a factor of 500 improvement in error sensitivity over an RTD.

However, the thermistor's high sensitivity to temperature does not come without a price. As previously shown in Figure 4-78, the temperature coefficient of thermistors does not decrease linearly with increasing temperature as with RTDs, and as a result linearization is required for all but the most narrow temperature ranges. Thermistor applications are limited to a few hundred degrees at best, because thermistors are also more susceptible to damage at high temperatures.

Compared to thermocouples and RTDs, thermistors are fragile in construction and require careful mounting procedures to prevent crushing or bond separation. Although a thermistor's response time is short due to its small size, its small thermal mass also makes it very sensitive to self-heating errors.

Thermistors are very inexpensive, highly sensitive temperature sensors. However, we have noted that a thermistor's temperature coefficient can vary, from $-44,000$ ppm/°C at 25°C, to $-29,000$ ppm/°C at 100°C. Not only is this nonlinearity the largest source of error in a temperature measurement, it also limits useful applications to very narrow temperature ranges without linearization.

As shown in Figure 4-79, a parallel resistor combination exhibits a more linear variation with temperature compared to the thermistor itself. This approach to linearizing a thermistor simply shunts it with a fixed, temperature-stable resistor. Paralleling the thermistor with a fixed resistor increases the linearity significantly. Also, the sensitivity of the combination still is high compared to a thermocouple or RTD. The primary disadvantage of the technique is that linearization is only effective within a narrow range. However, it is possible to use a thermistor over a wide temperature range, if the system designer can tolerate a lower net sensitivity, in order to achieve improved linearity.

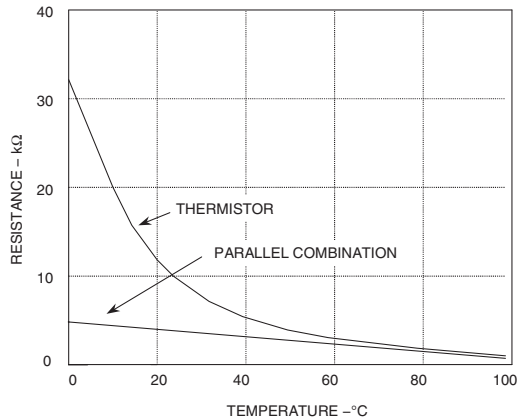


Figure 4-79: Linearization of NTC thermistor using a fixed shunt resistance

R, the value of the fixed shunt resistor, can be calculated from the following equation:

$$R = \frac{RT2 \cdot (RT1 + RT3) - 2 \cdot RT1 \cdot RT3}{RT1 + RT3 - 2 \cdot RT2} \quad \text{Eq. 4-11}$$

where $RT1$ is the thermistor resistance at $T1$, the lowest temperature in the measurement range, $RT3$ is the thermistor resistance at $T3$, the highest temperature in the range, and $RT2$ is the thermistor resistance at $T2$, the midpoint, $T2 = (T1 + T3)/2$.

For a typical 10 kΩ NTC thermistor, $RT1 = 32,650 \Omega$ at 0°C , $RT2 = 6,532 \Omega$ at 35°C , and $RT3 = 1,752 \Omega$ at 70°C . This results in a value of 5.17 kΩ for R. The accuracy needed in the associated signal-conditioning circuitry depends on the linearity of the network. For the example given above, the network shows a nonlinearity of $-2.3^\circ\text{C}/+2.0^\circ\text{C}$.

The output of the network can be applied to an ADC for digital conversion (with optional linearization) as shown in Figure 4-80. Note that the output of the thermistor network has a slope of approximately $-10 \text{ mV}/^\circ\text{C}$, which implies that an 8- or 10-bit ADC easily has more than sufficient resolution with a full scale range of 1 V or less. The further linearization can be applied to the data in the digital domain, if desired.

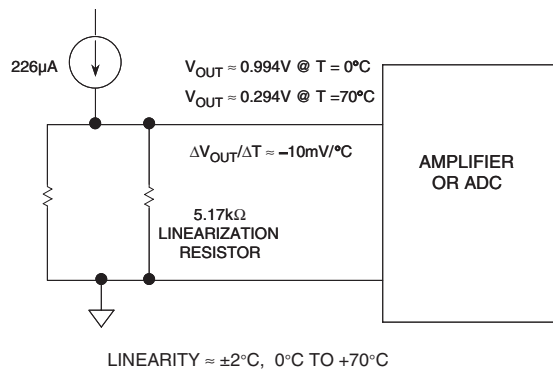


Figure 4-80: Linearized thermistor network with amplifier or ADC

Semiconductor Temperature Sensors

Modern semiconductor temperature sensors offer high accuracy and high linearity over an operating range of about -55°C to $+150^{\circ}\text{C}$. Internal amplifiers can scale the output to convenient values, such as $10\text{ mV}/^{\circ}\text{C}$. They are also useful in cold-junction-compensation circuits for wide temperature range thermocouples.

All semiconductor temperature sensors make use of the relationship between a bipolar junction transistor's (BJT) base-emitter voltage to its collector current:

$$V_{\text{BE}} = \frac{kT}{q} \ln\left(\frac{I_{\text{C}}}{I_{\text{S}}}\right) \quad \text{Eq. 4-12}$$

In this expression k is Boltzmann's constant, T is the absolute temperature, q is the charge of an electron, and I_{S} is a current related to the geometry and the temperature of the transistors. (The equation assumes a voltage of at least a few hundred mV on the collector, and ignores Early effects.)

If we take 'N' transistors identical to the first (see Figure 4-81) and allow the total current I_{C} to be shared equally among them, we find that the new base-emitter voltage applicable to this case is given by the equation

$$V_{\text{N}} = \frac{kT}{q} \ln\left(\frac{I_{\text{C}}}{N \cdot I_{\text{S}}}\right) \quad \text{Eq. 4-13}$$

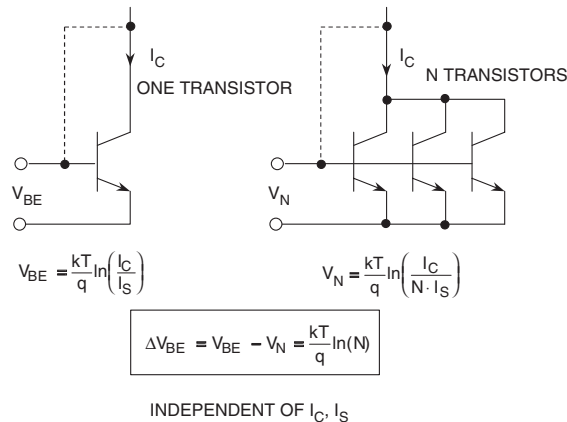


Figure 4-81: The basic relationships for BJT-based semiconductor temperature sensors

Neither of these circuits is of much use by itself, because of the strong temperature dependence of I_{S} . However, if we have equal currents flowing in one BJT, as well as the N similar BJTs, then the expression for the *difference* between the respective base-emitter voltages (or ΔV_{BE}) is proportional to absolute temperature, and it does not contain I_{S} .

This then leads to a far more useful relationship, developed as follows:

$$\Delta V_{\text{BE}} = V_{\text{BE}} - V_{\text{N}} = \frac{kT}{q} \ln\left(\frac{I_{\text{C}}}{I_{\text{S}}}\right) - \frac{kT}{q} \ln\left(\frac{I_{\text{C}}}{N \cdot I_{\text{S}}}\right)$$

$$\Delta V_{BE} = V_{BE} - V_N = \frac{kT}{q} \left[\ln\left(\frac{I_C}{I_S}\right) - \ln\left(\frac{I_C}{N \cdot I_S}\right) \right]$$

$$\Delta V_{BE} = V_{BE} - V_N = \frac{kT}{q} \ln \left[\frac{\left(\frac{I_C}{I_S}\right)}{\left(\frac{I_C}{N \cdot I_S}\right)} \right] = \frac{kT}{q} \ln(N)$$

This end result of this algebra is expressed in a single key equation, one worthy of restatement:

$$\Delta V_{BE} = \frac{kT}{q} \ln(N) \tag{Eq. 4-14}$$

As one can note, Eq. 4-14 contains only the transistor emitter area ratio N and T as variables. Since N is fixed within a given design, it can be the basis of a transducer for T measurement. The circuit as shown in Figure 4-82 implements the above equation, and is popularly known as the “Brokaw Cell,” after its inventor (see Reference 10).

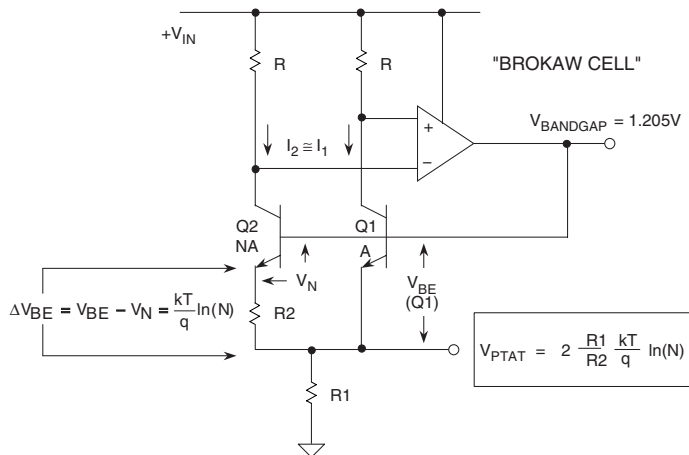


Figure 4-82: The “Brokaw Cell” is both a silicon bandgap voltage-based reference as well as a temperature sensor

The voltage $\Delta V_{BE} = V_{BE} - V_N$ appears across resistor R_2 , as noted. The emitter current in Q_2 is therefore $\Delta V_{BE}/R_2$. The op amp’s servo loop and the two resistors ‘ R ’ force an identical current to flow through Q_1 . The Q_1 and Q_2 currents are equal, and they are summed, flowing in resistor R_1 .

The corresponding voltage developed across R_1 is V_{PTAT} , a voltage proportional to absolute temperature (PTAT). This is given by:

$$V_{PTAT} = \frac{2R_1(V_{BE} - V_N)}{R_2} = 2 \frac{R_1}{R_2} \frac{kT}{q} \ln(N)$$

Within the circuit, a voltage labeled as V_{BANDGAP} appears at the base of Q1, and, as can be noted, is the sum of $V_{\text{BE(Q1)}}$ and V_{PTAT} . When this voltage is set by the design to be exactly equal to the bandgap voltage of silicon, it will then become independent of temperature. The voltage $V_{\text{BE(Q1)}}$ is complementary to absolute temperature (CTAT), and summing it with a properly proportioned V_{PTAT} from across R1 gives the desired end result; the bandgap voltage becomes constant with respect to temperature. Note that this assumes the proper choice of R1/R2 ratio and N, to make the summed voltage equal to V_{BANDGAP} , the silicon bandgap voltage (in this instance 1.205 V). This circuit has the virtues of dual application because of the above features. It is useful as a basic silicon bandgap temperature sensor, with either direct or scaled use of the voltage V_{PTAT} . It is also widely used a temperature stable reference voltage source, by suitable scaling of V_{BANDGAP} to standard outputs of 2.500 V, 5.000 V, and so forth.

Current and Voltage Output Temperature Sensors

The concepts used in the bandgap voltage temperature sensor discussion above can also be used as the basis for a variety of IC temperature sensors, with linear, proportional-to-temperature outputs, of either current or voltage.

The AD592 device shown in Figure 4-83 is a two-terminal, current output sensor with a scale factor of $1 \mu\text{A/K}$. This device does not require external calibration, and is available in several accuracy grades. The AD592 is a TO92 packaged version of the original AD590 TO52 metal packaged temperature transducer device (see Reference 11).

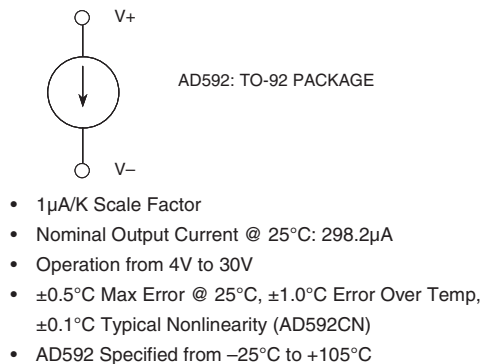


Figure 4-83: Current output absolute temperature sensor

The simplest operating mode for current mode temperature sensors is to load them with a precision resistor of 1% or better tolerance, and read the output voltage developed with either an ADC or a scaling amplifier/buffer. Figure 4-84 shows this technique with an ADC, as applicable to the AD592. The resistor load R1 converts the basic scaling of the sensor ($1 \mu\text{A/K}$) into a proportional voltage.

Choice of this resistor determines the overall sensitivity of the temperature sensor, in terms of V/K. For example, with a $1 \text{ k}\Omega$ precision resistor load as shown, the net circuit sensitivity becomes 1 mV/K . With a 5 V bias on the temperature sensor as shown, the AD592's full dynamic range is allowed with a $1 \text{ k}\Omega$ load. If a higher value R1 is used, higher bias voltage may be required, as the AD592 requires 4 V of operating headroom.

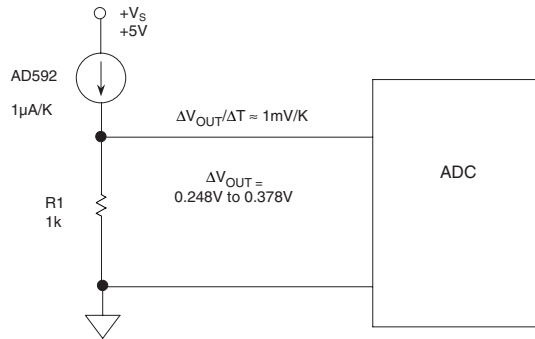


Figure 4-84: Current output temperature sensor driving a resistive load

The function just described is a Kelvin-scaled temperature sensor, so the ADC will be required to read the full dynamic range of voltage across R1. With an AD592, this span is from the range corresponding to -25°C (248 K) to 105°C (378 K), which is 0.248 V to 0.378 V. A 10-bit, 0.5 V scaled ADC can read this range directly with $\approx 0.5^{\circ}\text{C}$ resolution.

If a centigrade-scaled reading is desired, two options present themselves. For a traditional analog approach, the common terminal of the ADC input can easily be biased with a reference voltage corresponding to 0°C , or 0.273 V. Alternately, the 0°C reference can be inserted in the digital domain, with the advantage of no additional hardware requirement.

The AD592 is available in three accuracy grades. The highest grade version (AD592CN) has a maximum error @ 25°C of $\pm 0.5^{\circ}\text{C}$ and $\pm 1.0^{\circ}\text{C}$ error from -25°C to $+105^{\circ}\text{C}$, and a linearity error of $\pm 0.35^{\circ}\text{C}$. The AD592 is available in a TO-92 package.

With regard to stand-alone digital output temperature sensors, it is worthy of note that such devices do exist, that is ADCs with built-in temperature sensing. The AD7816/AD7817/AD7818-series ADCs have on-board temperature sensors digitized by a 10-bit $9\ \mu\text{s}$ conversion time switched capacitor SAR ADC. The device family offers a variety of input options for flexibility. The similar AD7416/AD7417/AD7418 have serial interfaces.

For a great many temperature sensing applications, a voltage mode output sensor is most appropriate. For this, there are a variety of standalone sensors that can be directly applied. In such devices the basic mode of operation is as a three-terminal device, using power input, common, and voltage output pins. In addition, some devices offer an optional shutdown pin.

The TMP35/TMP36 are low voltage (2.7 V to 5.5 V), SO-8 or TO-92 packaged voltage output temperature sensors with a 10 mV/°C scale factor, as shown in Figure 4-85. Supply current is below 50 μA , providing very low self-heating (less than 0.1°C in still air).

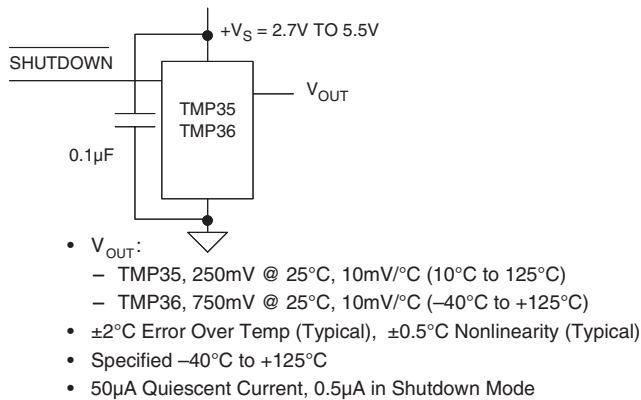


Figure 4-85: TMP35/36 absolute scaled voltage mode output temperature sensors with shutdown capability

Output scaling of this device family differs in range and 25°C offset. The TMP35 provides a 250 mV output at 25°C, and reads temperature from 10°C to 125°C. The TMP36 is specified from –40°C to +125°C, and provides a 750 mV output at 25°C. Both the TMP35 and TMP36 have an output scale factor of +10 mV/°C.

An optional shutdown feature is provided for the SO8 package devices, which reduces the standby current to 0.5 μA . This pin, when taken to a logic LOW, turns the device OFF, and the output becomes a high impedance state. If shutdown isn't used, the pin should be connected to +V_S.

The power supply pin of these voltage mode sensors should be bypassed to ground with a 0.1 μF ceramic capacitor having very short leads (preferably surface mount) and located as close to the power supply pin as possible. Since these temperature sensors operate on very little supply current and could be exposed to very hostile electrical environments, it is also important to minimize the effects of EMI/RFI on these devices. The effect of RFI on these temperature sensors is manifested as abnormal dc shifts in the output voltage due to rectification of the high frequency noise by the internal IC junctions. In those cases where the devices are operated in the presence of high frequency radiated or conducted noise, a large value tantalum electrolytic capacitor (>2.2 μF) placed across the 0.1 μF ceramic may offer additional noise immunity.

Ratiometric Voltage Output Temperature Sensors

In some cases, it is desirable for the output of a temperature sensor to be *ratiometric* with respect its supply voltage. A series of ADI temperature sensors have been designed to fulfill this need, in the form of the AD2210x series (see references 12–14). Of this series, the AD22103 illustrated in Figure 4-86 has an output that is ratiometric with regard its nominal 3.3 V supply voltage, according to the equation:

$$V_{\text{OUT}} = \frac{V_{\text{S}}}{3.3\text{V}} \times \left(0.25\text{V} + \frac{28\text{mV}}{^{\circ}\text{C}} \times T_{\text{A}} \right). \quad \text{Eq. 4-15}$$

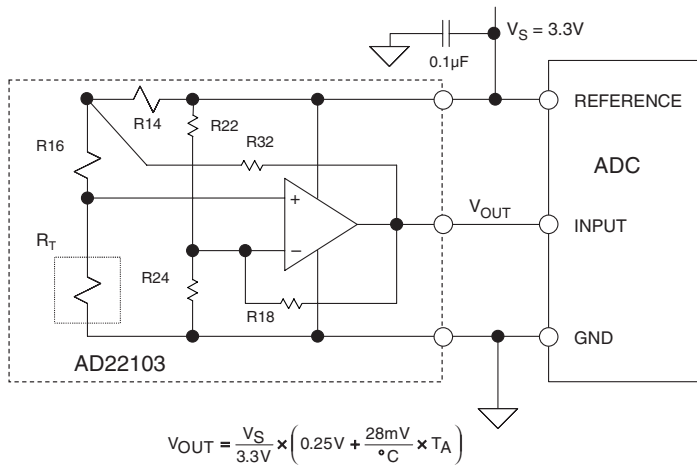


Figure 4-86: Ratiometric voltage output temperature sensors

Note also that the Figure 4-86 circuit uses the 3.3 V AD22103 power supply voltage as the reference input to the ADC. This step eliminates the need for a separate precision voltage reference source. Within a system, this key point potentially can have a positive impact.

Operation of the AD22103 is accomplished with an on-chip temperature sensing resistance R_T , which operates similarly to the RTD types discussed earlier in this section. This resistance is fed from a resistance network comprised of R14, R16, and R32. R14 and R16 provide a current drive component for R_T that is proportional to the supply voltage, a factor that gives the AD22103 a basic sensitivity that is proportional to the supply. R_T , like a classic platinum RTD, exhibits a nonlinear resistance versus temperature behavior. This nonlinear characteristic of R_T is corrected by a positive feedback loop, composed of R32 along with the Thevenin equivalent of resistances R14 and R16.

Gain scaling for the changing R_T output voltage is provided by the op amp negative feedback loop, R18, and the Thevenin equivalent of resistances R24 and R22. This references the gain network of the op amp to the supply voltage, instead of ground. The various resistance networks around the op amp are actively trimmed at temperature, to calibrate the sensor for its rated offset and scaling.

The net combination of these factors allows the device to behave in accordance with the relationship of Eq. 4-15. The AD22103 is specified over a range of 0°C to 100°C, and has an accuracy better than $\pm 2.5^\circ\text{C}$, along with a linearity better than $\pm 0.5\%$ of full scale, i.e., 0.5°C over 100°C.

Since the AD22103 is a single-supply part, the sensing of low temperatures necessarily involves a positive output offset. For example, for 3.3 V operation of this example, the output offset is simply the 0.25 V term of Eq. 4-15. Accordingly, the 0 to 100°C temperature span translates to an output swing of 0.25 V to 3.05 V.

Should it be desired, operation of the AD22103 device is also possible at higher supply voltages. Because of the ratiometric operation feature, this will necessarily involve a change to both the basic sensitivity and the offset. For example, in operating the AD22103 at 5 V, the output expression changes to:

$$V_{OUT} = \frac{V_S}{5V} \times \left(0.378V + \frac{42.42mV}{^\circ C} \times T_A \right) \quad \text{Eq. 4-16}$$

However, it should be noted that the fact that the AD22103 is ratiometric does *not* preclude operating the part from a fixed reference voltage. The nominal current drain of the AD22103 is 500 μ A, allowing a number of these sensors to be operated from a common reference IC without danger of overload (as well as other analog parts). For example, one such reference family is the REF19x series, which can supply output currents of up to 30 mA.

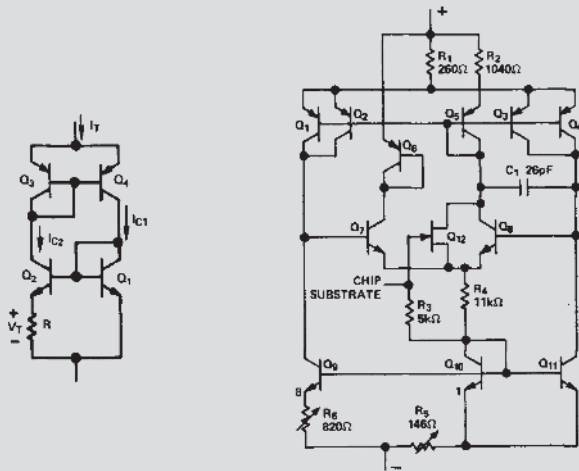
In addition to the above-described AD22103 3.3 V part, there is also a companion device, the AD22100. While basically quite similar to the AD22103, the AD22100 operates from a nominal 5 V power supply with reduced sensitivity, allowing operation over a range of -50 to $+150^{\circ}\text{C}$. Over this range the rated accuracy of the AD22100 is 2% or better, and linearity error is 1% or less.

References: Temperature Sensors

1. Ramon Pallas-Areny and John G. Webster, **Sensors and Signal Conditioning**, John Wiley, New York, 1991.
2. Dan Sheingold, Editor, **Transducer Interfacing Handbook**, Analog Devices, Inc., 1980, ISBN: 0-916550-05-2.
3. Sections 2, 3, Walt Kester, Editor, **1992 Amplifier Applications Guide**, Analog Devices, 1992, ISBN: 0-916550-10-9.
4. Sections 1, 6, Walt Kester, Editor, **System Applications Guide**, Analog Devices, 1993, ISBN: 0-916550-13-3.
5. Dan Sheingold, Editor, **Nonlinear Circuits Handbook**, Analog Devices, Inc., 1974.
6. James Wong, "Temperature Measurements Gain from Advances in High-precision Op Amps," **Electronic Design**, May 15, 1986.
7. OMEGA Temperature Measurement Handbook, Omega Instruments, Inc.
8. **Handbook of Chemistry and Physics**, Chemical Rubber Co.
9. Joe Marcin, "Thermocouple Signal Conditioning Using the AD594/AD595," **Analog Devices AN369**.
10. Paul Brokaw, "A Simple Three-Terminal IC Bandgap Voltage Reference," **IEEE Journal of Solid-State Circuits**, Vol. SC-9, No. 6, December, 1974, pp. 388–393.
11. Mike Timko, "A Two-Terminal IC Temperature Transducer," **IEEE Journal of Solid-State Circuits**, Vol. SC-11, No. 6, December, 1976, pp. 784–788.
12. Data sheet for **AD22103 3.3 V Supply, Voltage Output Temperature Sensor with Signal Conditioning**, www.analog.com.
13. Data sheet for **AD22100 Voltage Output Temperature Sensor with Signal Conditioning**, www.analog.com.
14. Adrian P. Brokaw, "Monolithic Ratiometric Temperature Measurement Circuit," **US Patent No. 5,030,849**, filed June 30, 1989, issued July 9, 1991.

Classic Cameo

AD590 Two-Terminal IC Temperature Transducer



AD590 basic (left), and complete schematics (right)

Designed by Mike Timko, based on an original Paul Brokaw concept,¹ the AD590^{2,3,4} current mode IC temperature transducer was introduced in 1977. The AD590 established early an elegant method of accurate temperature measurement, based upon fundamental silicon transistor operating principles. It has been in ADI production since introduction, along with such related ICs as the AD592 discussed within this chapter.

The references below discuss operation in great detail, but suffice it to say that in the basic structure (left) a voltage proportional to absolute temperature, V_T , appears across resistor R . This makes the current I_T drawn from an external source proportional to absolute temperature. In the full circuit (right), trimmed thin film resistors implement a calibrated scaling for I_T of $1\mu\text{A}/\text{K}$. Additional circuitry is added for startup and for increased accuracy, both with respect to applied voltage as well as against high temperature leakage.

A current-operated transducer such as this is quite convenient to operate, the output being impervious to long lead lengths, and also virtually noise-immune. The low scaling factor also makes the AD590 easy to operate on low voltage supplies without self-heating, yet high output impedance also holds calibration with higher applied voltages. Readout is simply accomplished with a single resistance, making a simple, two-component Kelvin-scaled thermometer possible.

- 1 Adrian P. Brokaw, "Digital-to-Analog Converter with Current Source Transistors Operated Accurately at Different Current Densities," **US Patent No. 3,940,760**, filed March 21, 1975, issued Feb. 24, 1976.
- 2 Mike Timko, "A Two-Terminal IC Temperature Transducer," **IEEE Journal of Solid-State Circuits**, Vol. SC-11, No. 6, December, 1976, pp. 784–788.
- 3 Mike Timko, Goodloe Suttler, "1 $\mu\text{A}/\text{K}$ IC Temperature-to-Current Transducer," **Analog Dialogue**, Vol. 12, No. 1, 1978, pp. 3–5.
- 4 Michael P. Timko, Adrian P. Brokaw, "Integrated Circuit Two Terminal Temperature Transducer," **US Patent No. 4,123,698**, filed July 6, 1976, issued October 31, 1978.